5-2017

Surface Modification of Pillar Array Systems for Chromatography and Fluorescence Enhancement

Danielle Ruth Lincoln
University of Tennessee, Knoxville, dlincol3@vols.utk.edu

To the Graduate Council:

I am submitting herewith a dissertation written by Danielle Ruth Lincoln entitled "Surface Modification of Pillar Array Systems for Chromatography and Fluorescence Enhancement." I have examined the final electronic copy of this dissertation for form and content and recommend that it be accepted in partial fulfillment of the requirements for the degree of Doctor of Philosophy, with a major in Chemistry.

Michael J. Sepaniak, Major Professor

We have read this dissertation and recommend its acceptance:

Christopher A. Baker, Robert J. Hinde, Dawnie W. Steadman

Accepted for the Council:
Dixie L. Thompson

Vice Provost and Dean of the Graduate School

(Original signatures are on file with official student records.)

Surface Modification of Pillar Array Systems for Chromatography and Fluorescence Enhancement

A Dissertation Presented for the
Doctor of Philosophy
Degree
The University of Tennessee, Knoxville

Danielle Ruth Lincoln
May 2017

For Mimi
and Grandpa

Acknowledgements

First and foremost, I would like to thank my research advisor, Dr. Michael Sepaniak. Beyond the incredible scope of knowledge and experience you have shared with me, I am enormously grateful for your guidance, encouragement, and above all your patience. I could not have made it to this point without you.

I would also like to acknowledge Dr. Nick Lavrik, for your mentorship and infinitely insightful input on this research. Additional thank yous to the exceptional staff at the Center for Nanophase Materials Sciences. Without your collaboration, a great deal of this work would not have been possible.

Thank you to the members of the Sepaniak research group, past and present. Tess, Jennifer, Nichole, Nahla, Ryan, and Rachel, I have learned so much from every one of you, in research and in life. You have been one of my most important support systems and I am proud to have worked alongside of you.

Finally, I would like to thank:

Drew, for keeping me together in some of my darkest moments, although you may not have known it, and for serving as a constant reminder that, as long as I keep my weight over my feet and pay attention to the lead given to me, I can do anything.

Liz and Richard, for your support and for opening your home to me when it turned out I couldn't get any writing done anywhere else. Also, my Heronskeep family, for being the home away from home I didn't know I needed.

My mom, dad, and brother, for being by first and loudest cheerleaders, and Ana and Jenn and Brittany for your unflinching belief that I could actually do this thing.

And Andrew. There are no words. I love you. Our future awaits us.

Abstract

Thin-layer chromatography offers many advantages in the world of chemical separations due to its ease of use, high sensitivity, range of applicability, and multiplex capability. However, this technique is succeptible to band broadening effects that limit its efficiency. Attempting to resolve these effects by decreasing particle size causes a decrease in mobile phase velocity which creates its own band broadening via longitudinal diffusion. However, pillar array systems on the micro- and nanoscale have been shown as useful analogues to thin-layer chromatography which mitigate the efficiency concerns associated with the method.

The work within this dissertation is concerned with the modification of pillar array surfaces for both chromatographic and spectroscopic purposes. The first aim is to increase the surface area of the pillars for chromatography by depositing porous phases such as petal-like carbon and porous silicon oxide. The usefulness of pillar arrays as separations systems is moderated by their limited native surface area. Increasing the surface area of a stationary phase can increase the retention of analyte by the system without negatively affecting its efficiency. While we found that petal-like carbon has several properties that made it unsuitable for these pillar array systems in their current form, porous silicon oxide showed great promise as a porous phase which increased the surface area of the pillars and the retention of analytes within them.

The second aim was to immobilize fluorescent molecules at the pillar surface for signal enhancement. Pillars in the nanoscale have been shown to exhibit a field effect which amplifies fluorescence signal. To this end, we developed wet chemistry methods to functionalize the pillar surface with two different immobilizing resins, one using a uranium-capturing compound, and the other a biotin-avidin complex to sequester DNA. In both cases, we created high-throughput methods which retained high sensitivity while using only minimal amounts of sample.

Table of Contents

1. Introduction to planar chromatography 1
   - 1.1 Thin layer chromatography: History and basic principle 2
   - 1.2 Discussion of stationary phases in planar chromatography 4
   - 1.3 Discussion of mobile phase and mobile phase flow 4
   - 1.4 Sample application 8
   - 1.5 Development method and detection 9
   - 1.6 Efficiency, the Van Deemter equation, and factors that affect band broadening 13
   - 1.7 Experimentally determined evaluation metrics 15
   - 1.8 Conclusions about thin layer chromatography 17
2. Introduction to nanopillars 18
   - 2.1 History and basic principle 19
   - 2.2 Efficiency, or Why we use pillar arrays for thin layer chromatography 19
   - 2.3 Design of deterministic pillars by photolithography 20
   - 2.4 Design of deterministic pillars by electron beam lithography 21
   - 2.5 Design of stochastic pillars 24
   - 2.6 Reactive ion etching 24
   - 2.7 Surface modification 26
   - 2.8 Conclusions about pillar arrays 28
3. Capillary driven transport and dispersion in hierarchically porous phases formed by conformal deposition of petal like carbon on silicon pillar arrays 29
   - 3.1 Abstract 30
   - 3.2 Introduction to carbonaceous stationary phases 30
   - 3.3 Fabrication and deposition of petal like carbon 31
   - 3.4 Solvent transport studies 32
   - 3.5 Possible form change with increasing thickness and preliminary
   - 3.6 surface area calculations 36
   - 3.7 Preliminary solute transport using a two-phase system 36
   - 3.8 Conclusions about petal like carbon 37
4. Retention in porous layer pillar array planar separation platforms 39
   - 4.1 Abstract 41
   - 4.2 Introduction 41
   - 4.3 Experimental 43
   - 4.4 Results and Discussion 49
   - 4.5 Conclusion 61
5. Surface modification of pillar arraysto enhance fluorescence detection of uranium and DNA 63
   - 5.1 Abstract 64
   - 5.2 Introduction 64

5.3 Experimental....66
5.4 Results and Discussion....74
5.5 Conclusion....81
6. Conclusion....82
6.1 Concluding Remarks....83
References....85
Appendix....91
Vita....95

List of Tables

Table 1.3.1 Polarity Indices of Common Pure Solvents as Derived from Rohrschneider Data.....7
Table 4.3.1 Surface area factor increase due to PSO, determined by fluorescence....48

List of Figures

Figure 1.4.1 Image of spotted samples in various stages of concentration/drying. On the left is the first stage, wherein the droplet is in the Cassie state and sitting on top of the pillars. Next to it is the second stage, wherein the droplet is in the Wenzel state and has begun to sink into the pillars. Note that the contact angle dramatically increases when this transition occurs 10

Figure 1.5.1 Illustrations of the two development chambers used in this study (not to scale). The chamber on the left was used for one-dimensional development on 1 cm x 3 cm arrays and the chamber on the right was used for two-dimensional development on 3 cm x 3 cm arrays. Both chambers featured a piston to raise and lower the array into the solvent well, and a sponge to facilitate even vapor saturation..... 12

Figure 2.3.1 Illustration of the photolithographic process used in this work..... 22

Figure 2.6.1 Schematic of an RIE chamber using SF_5 for etching 25

Figure 2.6.2 At the top is an illustration of the Bosch process, which when repeated can produce pillars such as shown at the bottom, with high aspect ratios and characteristic scalloped sidewalls 27

Figure 3.3.1 Photolithographically-fabricated pillars before application of any coating (**A**), after application of PLC (**B**), with inset depicting the characteristic fuzziness of the PLC fibers, and after overcoating with SiO_2 (**C**) 33

Figure 3.4.1 Relationship of solvent front movement to time for various solvents on a PLC array and a traditional C18 array 35

Figure 3.6.1 Coumarin (green) and sulforhodamine (red) pre- and post-development on a SiO_2-coated PLC array with 100% isopropanol. The initial spot, shown on the left, was imaged under green (top) and blue (bottom) excitation to visualize the sulforhodamine and coumarin, respectively. On the developed array, sulforhodamine was visible below and to the left of the coumarin, indicating that it was less retained 38

Figure 4.3.1 **A** pictorializes the fabrication sequence, which begins with a silicon wafer substrate that is photolithographically patterned. The wafer is then etched with anisotropic DRIE and coated with a thin layer of PSO via PECVD. **B** shows an SEM of a pillar before and after deposition of 50 nm PSO, with a close-up of the PSO granules included. **C** describes the three-component effective medium model used to determine void fraction in PSO, composed of SiO_2, void, and H_2O..... 44

Figure 4.4.1 **A** shows the retention of coumarin 153 versus the solvent polarity index of the mobile phase used. Blue squares indicate ethanol as the organic modifier, the orange triangle indicates methanol, and the green circle indicates isopropanol. **B** shows the ln(k') of

coumarin 153 versus the percent of organic modifier (ethanol) for 50 nm PSO, 100 nm PSO, and 150 nm PSO 52
Figure 4.4.2 Cursory evaluation of efficiency trends, given by plate height (H), of the arrays with three different thicknesses of PSO (50 nm, 100 nm, and 150 nm) using Coumarin 152, shown as a function of mobile phase ratio (ethanol:water). Although the individual values are somewhat inflated, the overall trends depicted reflect the decrease in efficiency as PSO thickness is increased 57
Figure 4.4.3 **A** depicts the spot locations of the dye in the dye mixture, as separated on 4 different arrays (100 nm PSO C4 functionalized, 50 nm C4 functionalized, 150 nm PSO C4 functionalized, and 50 nm PSO C18 functionalized) relative to one another, with the length of the line corresponding to the full 3 cm length of the array. The initial spot location is shown in black, the location of the Coumarin 153 is shown in green, the location of the Coumarins 120 and 2 are shown in blue, and the location of the Sulforhodamine, which is unretained, is shown in red. **B** is a graph of the retardation factors of the different dyes on the different arrays.....58
Figure 4.4.4 On the left is a diagram of the NBD-amine locations after development in the first (40:60 EtOH:H_2O) and second (40:60 EtOH:H_2O with 0.038 M $AgNO_3$) dimensions. In the first dimension, in order from most to least retained, are heptylamine (1, red), hexylamine and 1-amino-5-hexene coeluted (2, blue), pentylamine (3, green), and butylamine and propylamine coeluted (4, orange). In the second dimension, the coeluted amines are separated and we see, from most to least retained, heptylamine (5, red), hexylamine (6, blue), pentylamine (7, green), 1-amino-5-hexene (8, blue), butylamine (9, orange), and propylamine (10, orange). There is a staggered effect—most notable for hexylamine and 1-amino-5-hexene—due to a lateral vector in the movement of the mobile phase in the second dimension. **A** shows an image of NBD-heptylamine after development in the first dimension. **B** shows an image of NBD-pentylamine and NBD-1-amino-5-hexene after development in the second dimension, superimposed with the plot profiles of the two spots to show the resolution between the two spots 60
Figure 5.3.1 Layout of the EBL arrays used is shown in (**A**), with an SEM image of the created arrays in (**B**). Inset (**C**) shows a close-up of one of the 10 pillar x 10 pillar arrays within this larger array of arrays.....67
Figure 5.3.2 Functinalization sequence for immobilization of DNA on the pillar surface. Pillars are acid bathed (**1**), then functionalized with APTES (**2**). They are biotinylated by addition of sulfo-NHS-biotin (**3**) and addition of avidin (**4**) completes the extraction surface. When DNA solutions are introduced (**5**), the biotinylated DNA strands are bound by the avidin-functionalized pillars 72

Figure 5.4.1 Fluorescence microscope images of EBL pillars functionalized with APTES and soaked with FITC to determine optimum pillar width and PSO thickness are shown at the top, with pillar width increasing down the array, every other pillar in increments of 10 nm, from 60 nm to 100 nm. Below that are the plot profiles depicting fluorescence intensity for the 10 pillar x 10 pillar arrays pictured 75
Figure 5.4.2 Depiction of 100 and 200 ppm uranyl spotted on CMPO (top) and C4 (bottom) arrays, pre-rinse (left) and post-rinse (right) 77
Figure 5.4.3 Fluorescence microscope images of uranyl spotted on dewet arrays functionalized with CMPO are shown in (**A**) with corresponding heat maps below, where redder color indicates greater fluorescence signal intensity. Concentration increases from left to right: blank, 1 ppm, 25 ppm, 50 ppm, 75 ppm, 100 ppm, and 200 ppm. (**B**) shows the calibration curve for these samples. The blue circles represent the images shown here, where the curve exhibits linearity. The orange triangles represent the signals measured for 300 ppm, 400 ppm, and 500 ppm, where oversaturation of signal caused the intensity to level out 78
Figure 5.4.4 Fluorescent images of sample areas on pillar arrays functionalized for DNA immobilization and soaked with one of the four DNA solutions are shown in (**A**). Sample areas are shown pre- (top) and post- (bottom) rinse. (**B**) graphs the fluorescence intensity measured for each of these eight samples.....80
Figure A-1 Depiction of the model used to calculate surface area increase.....94

List of Abbreviations

TLC	Thin layer chromatography
HPTLC	High-performance thin layer chromatography
UTLC	Ultra-thin layer chromatography
NP	Normal phase
RP	Reverse phase
R_f	Retardation factor
ε^0	Solvent strength parameter
P’	Polarity index
F	Volume fraction of solvent
S_f	Distance traveled by the solvent front
k	Proportionality constant
t	Time
K_0	Permeability constant
d_p	Particle diameter
γ	Surface tension of the mobile phase
η	Viscosity of the mobile phase
θ	Contact angle of the mobile phase on the stationary phase
μ_f	Velocity of the solvent front
H	Theoretical plate height
A	Van Deemter A term for eddy diffusion
B	Van Deemter B term for longitudinal diffusion
C	Van Deemter C term for resistance to mass transfer
D_M	Diffusion coefficient of the mobile phase
d_f	Film thickness of the stationary phase
C_S	Van Deemter term for resistance to mass transfer in the stationary phase
C_M	Van Deemter term for resistance to mass transfer in the mobile phase
S_s	Distance between a developed band and the initial spot
S_0	Distance between the initial spot and the base of the plate
N	Number of theoretical plates
L	Distance traveled by the developed band
w_f	Band width after development
w_i	Initial width of the spot before development
σ	One-fourth the width of a developed band
N_c	Peak capacity
σ	Average standard deviation of the peaks
EBL	Electron beam lithography
CAD	Computer Aided Design
DNA	Deoxyribonucleic acid
ICP	Inductively coupled plasma
RIE	Reactive ion etching
RF	Radio frequency
DRIE	Deep reactive ion etching
PECVD	Plasma enhanced chemical vapor deposition

PLC	Petal-like carbon
PGC	Porous graphitic carbon
PSO	Porous silicon oxide
HPLC	High performance liquid chromatography
ORNL	Oak Ridge National Laboratory
EtOH	Ethanol
NMP	N-methyl-2-pyrrolidone
C18	Octadecyltrichlorosilane
L	Distance the solfent front traveled
k_0	Bed permeability
BET	Brunauer-Emmett-Teller (analysis)
2D	Two-dimensional
SEM	Scanning electron microscopy
C4	N-butyldimethylchlorosilane
SIE	Spectroscopic imaging ellipsometer
RH	Relative humidity
APTES	3-Aminopropyltriethoxysilane
FITC	Fluoresceinisothiocyanate
NBD	7-Chlor-4-nitrobenzofurazan
φ	Volume fraction
k’	Capacity factor
S	Solvent strength
φ	Fraction of organic modifier
SPE	Solid phase extraction
CMPO	N, N-diisobutyl-2-(octyl(phenyl)-phosphoryl) acetamide
DW	Dewetted
TEOS	Tetraethyl orthosilicate
THF	Tetrahydrofuran
NHS	N-hydroxysuccinimide
PBS	Phosphate buffered saline
ssDNA	Single-strand DNA
TE	Tris-EDTA buffer
EtBr	Ethidium bromide
V_{PSO}	Volume of PSO
V_{porous}	Volume of PSO that is not void
$V_{1sphere}$	Volume of one sphere
$N_{spheres}$	Number of spheres
A_{porous}	Surface area of all the spheres
$A_{1sphere}$	Surface area of one sphere
R_g	Surface roughness factor
A_{pillar}	Surface area of a pillar

Chapter 1

Introduction to Planar Chromatography

1.1 – Thin Layer Chromatography: History and Basic Principles

Thin layer chromatography (TLC) is a form of planar chromatography in which a thin layer of stationary phase is applied to a solid support, across which the mobile phase moves by capillary action. It is one of the most popular and widely used separations techniques due to ease of use, broad applicability, and relative low cost and multiplex capabilities compared to other techniques. It may be used to confirm the purity of a sample, determine components in a mixture, or even quantitatively determine the amount of an analyte present.

TLC was first described in 1938 by Nikolai Izmailov and Maria Shraiber, although they referred to it as the "drop-chromatographic method." However, it wasn't until the work of Miller, Kirchner, and Keller in 1951 that the method began to attract attention.[1–3] Then in 1958, Stahl finally described an efficient method for reproducibly preparing the plates and gave the method its current name, resulting in a significant increase in its popularity.[4]

In the TLC seen today, thin layers of a sorbent material (such as silica gel, cellulose, or alumina) are applied as a coating to a solid support such as a glass slide. The sample to be separated is applied to the base of the plate, generally by spotting, and the plate is then sealed into a saturated development chamber containing a well of a small amount of the mobile phase of choice. The base of the plate is allowed to come into contact with the mobile phase, which begins to wick up the plate by capillary action in a process known as development. Different compounds within the sample have different affinities for the stationary phase and are separated by differentially adsorbing onto it. An analyte with a higher affinity for the stationary phase will spend more time adsorbed to it, and thus be more retained.

After the mobile phase has traveled a designated distance, the plate is removed from the development chamber and allowed to dry. Once dried, the individual spots may be identified by viewing under a UV light, by fluorescence, or by spraying with a reagent.[5]

Generally, it may be said that chromatographic efficiency and speed increase with decreasing particle size. As such, developments in TLC technology have largely focused on methods to reduce particle size. High-performance thin layer chromatography (HPTLC) is characterized by particle sizes of 5-6 microns and an overall layer thickness of 100-250 microns. This may be compared to traditional TLC, which has particles sizes of 10-12 microns and an overall layer thickness of 250-1000 microns.[6] HPTLC also exhibits shorter development distances and faster development times than traditional TLC, and is frequently combined with methods for spot automation or software controlled sample analysis, allowing for more quantitative analysis.

Other, more specialized methods involving micro machining have been used for the development of ultra-thin layer chromatography (UTLC) since 2001. The first UTLC plates were made by coating a glass substrate with a monolithic silica layer 10 μm thick containing macropores of 1-2 μm to minimize flow resistance and mesopores of 3-4 nm to optimize retention.[7,8] Subsequent progress has been made in the area by Brett and Olesik.[9–12] Bezuidenhout and Brett have worked with glancing-angle deposition to create silicon nanocolumns 1-7 μm thick and 500 nm in diameter engineered into shapes such as helices, spirals, vertical posts, and zig zags.[9] To address the complexity of this method, Clark and Olesik developed a technique to quickly and cheaply create UTLC plates using an electrospinning method, resulting in a stationary phase composed of nanofibers with tunable diameters and mat thicknesses.[12] The work presented in this dissertation uses lithography to create micro- and nanopillar arrays for use in UTLC.

1.2 – Discussion of Stationary Phases in Planar Chromatography

Stationary phases in chromatography may be classified as either normal phase (NP) or reverse phase (RP). Normal phase systems are characterized as having a hydrophilic stationary phase and using one or more relatively hydrophobic or nonpolar solvents in the mobile phase. By contrast, reverse phase systems have hydrophobic stationary phases and use one or more relatively hydrophilic or polar solvents in the mobile phase. Normal phase systems were used for much of the original work in liquid and planar chromatography, and many traditional TLC plates used today still function as normal phase systems. However, reverse phase chromatography has grown in popularity due to the ability of the system to separate highly polar compounds and allow for the use of water as one of the mobile phase components.

The most common stationary phase in TLC is silica gel, a polar sorbent which is prepared by combining the silica spheres with a binder, making it into a slurry, and spreading it onto the solid support. Common binders include calcium sulfate, starch, or polymers, and they are used to produce a stable layer that will not readily flake off during use. However, binders may also be undesirable when they interfere with development or visualization, as some binders are soluble in aqueous solvents, some are not stable at very high temperatures, and some are not suitable for use with chemical-reaction-based visualization methods.[5] Other common NP stationary phase materials include cellulose, alumina, polyamide, kieselguhr, and magnesium oxide.[6] Silica gel, however, has the advantage of being able to be easily modified through silane chemistry to create a nonpolar phase for use in a RP system.

1.3 – Discussion of Mobile Phase and Mobile Phase Flow

Solvent systems are chosen such that they adequately wet the mobile phase, dissolve the analytes, are selective to the analytes used in the separation, and, when used, produce retardation

factor (R_f, discussed later in 1.7) values that are between 0.3 and 0.7.[5,6] Furthermore, when more than one solvent is used, as often happens, they should be as different as possible while remaining miscible. In NP systems, this usually takes the form of a nonpolar organic hydrocarbon modified with a polar organic solvent such as an alcohol or ester.[6] In RP systems, the solvent base is most frequently water, modified with a polar organic compound such as methanol, acetonitrile, or tetrahydrofuran.[6] Care must be taken in the case of RP systems, as mobile phases containing more than 25% water may have difficulty wetting the stationary phase, resulting in the inability of the solvent to move up the plate. Other factors such as viscosity, vapor pressure, toxicity, and stability should also be considered during system selection.

Solvent systems are generally chosen via a combination of literature review and trial-and-error. This method is frequently tedious, however, and so there has been some work to create models to assist in selection. The eluotropic series for solvent selection was first developed by Trappe and organizes pure solvents by their solvent strength parameter (ε^0) for a particular adsorbent.[13] The magnitude of ε^0 is the adsorption energy of the solvent per unit of standard sorbent. The greater the strength of the mobile phase, the greater the interaction with the sorbent, and the greater the mobility of the solute (i.e. the solute will be less retained). Once a solvent system with the proper strength to obtain the desired mobility of solute has been discovered, selectivity of the system may be tuned by selecting solvents with the same strengths, but different solute-solvent interactions. Snyder applied this idea to the concept of the polarity index (P'), which provided a more systematic approach wherein the volumes of different solvents necessary to reach the desired R_f may be determined.[14] Total P' may be calculated using the following equation:

$$P' = \sum_i F_i P'_i \qquad [1.3.1]$$

wherein F_i represents the volume fraction of the ith pure solvent in the mixture with a polarity index P'_i. Table 1.3.1 lists the polarity indices of some common pure solvents as given by Snyder.

The leading model of TLC considers the sorbent bed to be comprised of interconnected capillaries of varying diameter.[6] Before development begins, this bed is dry, and as the mobile phase is applied to one end, it is drawn across the bed by capillary action. As a result, the solvent front velocity is greater than that of the bulk mobile phase. This effect may be minimized by increasing the homogeneity of the bed, but even the most homogeneous sorbent layer would still exhibit a gradient of solvent volume, decreasing from the reservoir to the solvent front. There is evidence that this phase ratio gradient may actually contribute to sharper bands in UTLC performed with nanopillar arrays.[15] The distance that the solvent moves (S_f) over time t may be calculated using the equation

$$S_f = \sqrt{kt} \qquad [1.3.2]$$

wherein k is the proportionality constant and is described as

$$k = \frac{2K_0 d_p \gamma}{\eta \cos\theta}. \qquad [1.3.3]$$

In this equation, K_0 is the permeability constant, d_p is the particle diameter, γ is the surface tension of the mobile phase, η is the viscosity of the mobile phase, and θ is the contact angle of the mobile phase on the stationary phase (a value that is almost always 0 in TLC, so the cos θ value is considered to be unity). An equation for the velocity of the solvent front (μ_f) can also be written using these terms, as shown in equation 1.3.4.

$$\mu_f = \frac{k}{2S_f} \qquad [1.3.4]$$

Table 1.3.1 Polarity Indices of Common Pure Solvents as Derived from Rohrschneider Data[6,14]

Solvent	P'	Solvent	P'
N-Hexane	0.00	Ethanol	5.2
Carbon disulfide	1.00	Pyridine	5.3
Triethylamine	1.8	Acetone	5.4
Toluene	2.3	Ethylene glycol	5.4
Diphenyl ether	2.8	Benzyl alcohol	5.5
Benzene	3.0	Methylformamide	6.2
Methylene chloride	3.4	Acetic acid	6.2
t-Butanol	3.9	Acetonitrile	6.2
Tetrahydrofuran	4.2	N-Methyl-2-pyrrolidone	6.5
Ethyl acetate	4.3	Methanol	6.6
Isopropanol	4.3	Formamide	7.3
Chloroform	4.4	Water	9.0

Here, it can be seen that the mobile phase velocity is directly proportional to particle diameter and surface tension of the mobile phase and inversely related to the viscosity of the mobile phase. It also is apparent that the mobile phase velocity is not constant, and in fact decreases as development proceeds and the solvent front distance is increased.

Additionally, other undesirable effects must be taken into consideration when discussing mobile phase flow in TLC. Notably, some evaporation occurs at the solvent front, and when the mobile phase is composed of a mixture of liquids, the most volatile solvent will preferentially evaporate, creating a gradient of solvent composition across the bed. This is exacerbated by the preferential adsorption of the most polar solvent in the mixture onto the stationary phase.

1.4 –Sample Application

To achieve good chromatographic resolution and sensitive detection, the shape, size, and reproducibility of applied sample spots is of great importance. Spots that are too concentrated or nonuniform will give poor separation, as the mobile phase solvent will flow through the point of least resistance and travel around the spot instead of through it evenly, creating separated spots that are unsymmetrical after development.[5] Moreover, spots tend to diffuse and spread somewhat as they migrate further up the plate, and so the initial spot diameter should be as small as possible. Overloaded or too-large spots can result in significant tailing, the ends of which will overlap other spots on the plate and ruin the resolution.[5]

A variety of techniques and apparatuses have been used for sample application. Overall, these methods may be divided into manual and automatic methods. Manual methods generally consist of applying the sample by hand using a capillary or micropipette. Unfortunately, these methods suffer in reproducibility, as errors such as the creep back effect, the deposition of additional unwanted sample when spotting by contact (also known as capillation), and simple

operator experience can significantly affect the amount of sample spotted.[16] Automatic methods include apparatuses which hold many disposable capillaries at once, sample streak applicators, and syringe pumps. These methods do not necessarily guarantee small sample spots, only that the application will be reproducible. However, significant advancements have been made in the creation of automatic applicators for HPTLC. Morlock et al. have developed a method for using modified inkjet printer cartridges to deliver spots as small as 0.45 mm, and Fenimore and Meyer developed a method for contact spotting which can deliver a spot as small as 0.1 mm.[11,17]

The spotting method developed for the work in this dissertation takes advantage of the superhydrophobic nature of the pillar arrays. The micro- and nanoscale features, coupled with the hydrophobic carbon stationary phase with which they are coated results in a surface on which the sample may be spotted and allowed to concentrate and dry to a sub-mm size. When a suitable methanol/water mix is used in the sample solution, the droplet transitions from a Cassie state, where it is sitting on top of the pillars, to a Wenzel state, where it descends into the pillars.[18] This transition may be seen in Figure 1.4.1.

1.5 – Development Method and Detection

The majority of TLC development is done by allowing the mobile phase to travel up the plate, which is standing in a suitably-sized development chamber containing a reservoir of the mobile phase. Development may also occur horizontally, wherein the bottom of the plate is allowed to touch a wick saturated with the mobile phase, thus beginning solvent migration. In both cases, one of the most important considerations is chamber saturation, as unsaturation can cause unsymmetrical flow and exacerbate the phase ratio existing at the solvent front due to evaporation.

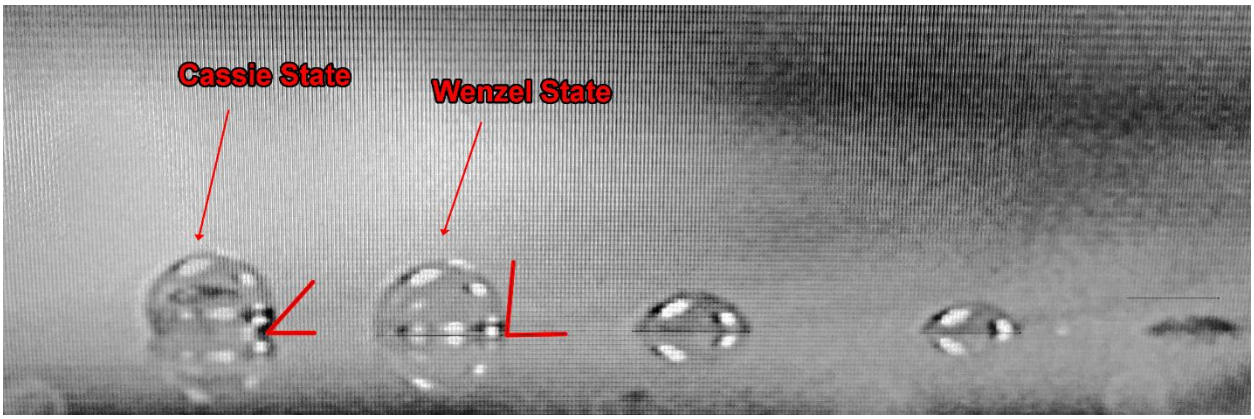

Figure 1.4.1: Image of spotted samples in various stages of concentration/drying. On the left is the first stage, wherein the droplet is in the Cassie state and sitting on top of the pillars. Next to it is the second stage, wherein the droplet is in the Wenzel state and has begun to sink into the pillars. Note that the contact angle dramatically increases when this transition occurs.

For the system described in this dissertation, two TLC chambers were constructed to assure suitable size for the arrays used. For the 1 cm x 3 cm arrays used for one-dimensional separations, a chamber was constructed using a dram vial with a sponge on the back wall to facilitate saturation and a piston to which the array could be attached such that it could be lowered at will into the mobile phase reservoir. For the 3 cm x 3 cm arrays used for two-dimensional separations, a similar chamber was constructed using glued microscope slides. An illustration of the two chambers is shown in Figure 1.5.1.

Spot detection in TLC is based largely upon natural color, absorbance, and florescence, or on the use of reagents to facilitate a color-changing chemical reaction. The former methods rely on the native fluorescence or phosphorescence of the analytes, or else use a fluorescent stationary phase on which the non-fluorescing samples will appear as dark spots on a bright background. The latter methods generally involve spraying the developed plate with a reagent, such as sulfuric acid. Unfortunately, these methods are destructive to the sample, whereas fluorescence methods allow for the samples to be subsequently transferred to different media for futher analysis if desired. Work has also been done coupling TLC to alternative detection methods. The spots may be excavated from the substrate and extracted, with the extract then available to be run through the desired instrumentation. For instance, Walworth et al. were able to use a liquid microjunction to couple developed HPTLC plates to a mass spectrometer for detection.[19]

In this research, a fluorescence microscope was used for both qualitative and quantitative detection.

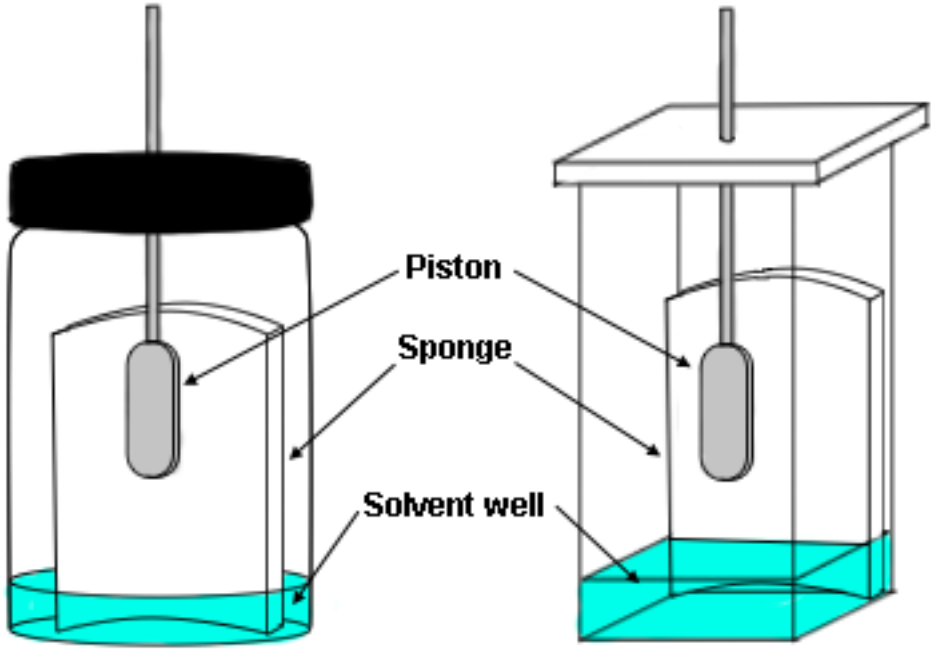

Figure 1.5.1: Illustrations of the two development chambers used in this study (not to scale). The chamber on the left was used for one-dimensional development on 1 cm x 3 cm arrays and the chamber on the right was used for two-dimensional development on 3 cm x 3 cm arrays. Both chambers featured a piston to raise and lower the array into the solvent well, and a sponge to facilitate even vapor saturation.

1.6 – Efficiency, the Van Deemter Equation, and Factors that Affect Band Broadening

Plate height, H, is a measure of the efficiency of a chromatographic system. It is independent of column length, and a small value for H is associated with a narrow solute band, and therefore high efficiency. While a great variety of complex factors contribute to plate height, it can generally be summarized by the van Deemter equation as a function of average linear mobile phase velocity, μ.

$$H = A(d_p) + \frac{B(D_M)}{\mu} + \left[C_s(d_f^2) + C_M\left(\frac{d_p^2}{D_M}\right)\right]\mu \qquad [1.6.1]$$

In this equation, the A, B, and C terms represent three effects that contribute to band broadening, and are functions of the particle diameter (d_p), the diffusion coefficient of the mobile phase (D_M), the film thickness of the stationary phase (d_f), and both particle diameter and the diffusion coefficient of the solute in the mobile phase, respectively. These three terms must be minimized in order to maximize efficiency.

The A term in the van Deemter equation deals with a phenomenon known as eddy diffusion. As identical molecules travel through the stationary phase, even if we assume that they start from the same initial position (as in an infinitesimally small spot), they will take differing paths through the sorbent and therefore travel different distances. Molecules that travel more direct paths will appear less retained than molecules that take a meandering path, resulting in band broadening.[6] The A term is minimized by decreasing particle size or by increasing packing order.

The B term in the van Deemter equation describes longitudinal diffusion. Molecules will, over time, diffuse naturally from areas of high concentration to areas of low concentration.

Thus, the more time that a solute spends on the column, or traveling up a chromatographic plate, the wider the spread of the resulting peak. The B term may be minimized by decreasing the diffusion coefficient (which is why the B term is less significant in liquid chromatography compared to gas chromatography), or, more practically, by increasing the mobile phase velocity. A high velocity will decrease the overall time the separation takes, and therefore decreases the amount of time solutes have to diffuse. This is reflected in the van Deemter equation by the division of the B term by μ.

The C term in the van Deemter equation is related to resistance to mass transfer, and can be further separated into C_s (resistance to mass transfer in the stationary phase) and C_M (resistance to mass transfer in the mobile phase) terms. Resistance to mass transfer in the stationary phase concerns the transfer of solute into and out of the stationary phase, or sorption and desorption. While the fraction of solute molecules adsorbed onto the stationary phase do not move, the solute molecules still in the mobile phase travel ahead, thus broadening the overall zone of molecules. The faster that the transition between sorbed and desorbed occurs, the less broadening that occurs. Because of this, the C_S term is minimized by decreasing the film thickness of the stationary phase.

In contrast, the resistance to mass transfer in the mobile phase is caused by the variation of mobile phase velocities as the solvent travels through a column (or up a plate, in the case of TLC). That is to say, a parabolic flow profile is representative of a mobile phase that does not move at the same speed in all places, and solute particles that spend more time in slower-moving zones will trail behind their counterparts in faster-moving zones, creating band broadening. This discrepancy is lessened by faster lateral diffusion, and thus the C_M term is inversely proportional to D_M. Likewise, the C_M term is lessened by decreasing the interstitial spaces between particles,

which in traditional TLC is determined by particle size—the smaller the particle size, the smaller the interstitial spaces. However, in pillar array systems the particle size and the interstitial spaces can be independently controlled, and studies on "closing the gap" between pillars have indeed determined that a smaller gap size is indicative of a more efficient system.[20]

In TLC, the C_M term is generally large due to the small D_M of solutes in the liquid mobile phase. While this is traditionally balanced in HPLC by using smaller diameter particles, this solution becomes more complicated in TLC because the drop in flow rate with migration distance becomes greater with finer particles. This decrease in μ is significant enough that it can offset the small D_M and longitudinal diffusion (the B term) begins to become substantial. The decrease in efficiency by using coarser particles can be somewhat mitigated by developing over a long distance, that can quickly become impractical.

1.7 – Experimentally Determined Evaluation Metrics

One of the most commonly used metrics in planar chromatography is the retardation factor, R_f, given by

$$R_f = \frac{S_s}{S_f - S_0} \qquad [1.7.1]$$

where S_s is the distance between the developed band and the initial spot, S_f is the distance traveled by the solvent front, and S_0 is the distance between the initial spot and the base of the plate. This metric is useful because it describes the movement of the analyte across the plate relative to other analytes, can be used to identify the analyte when compared to a standard, and can allow comparisons not only between plates, but also between planar and column chromatography.[6] When choosing development parameters, an R_f between 0.3 and 0.7 is

generally desired because the best resolution may be obtained in the middle third of the chromatographic region.[5]

As discussed in the previous section, plate height is a common parameter used to discuss the efficiency of a system. As the parameters in the van Deemter equation can be difficult to measure empirically, plate height can also be calculated experimentally by first calculating the number of plates (N):

$$N = 16\left(\frac{L}{w_f - w_i}\right)^2 \qquad [1.7.2]$$

where L is the distance traveled by the developed band, w_f is the band width after development, and w_i is the initial width of the spot before development. This can then be used to calculate H using

$$H = \frac{L}{N} \qquad [1.7.3]$$

In cases where the initial spot is much smaller than the developed band, or in cases where the initial spot may be assumed to be infinitesimally small to prevent absurd values of H (as in cases where the final band has experienced a concentrating effect, as observed by Kirchner et al)[21], this equation may be simplified to

$$H = \frac{\sigma^2}{L} \qquad [1.7.4]$$

where σ represents one-fourth the width of a developed band.

A chromatographic system may also be discussed in terms of the number of spots that may be resolved, also known as peak capacity (N_c). This can be experimentally determined using the equation put forth by Giddings,[22]

$$N_c = \frac{L}{4\sigma} \qquad [1.7.5]$$

where L is the distance across which peaks may be distributed and σ is the standard deviation of the peaks. Although it should be noted that in real-world samples, the actual peak capacity is typically only 18% of this theoretical value.[22] This value is particularly useful when considering the gain in chromatographic capability obtained when using two dimensions.

1.8 – Conclusions about Thin Layer Chromatography

Thin layer chromatography offers many advantages in its ease of use, high sensitivity, range of applicability, and multiplex capability compared to other chromatographic techniques. However, it suffers first in efficiency and second in reproducibility. The relatively large particle sizes and lack of uniformity commonly found in TLC result in mass transfer-related band broadening, and attempting to lessen it by reducing particle size causes a decrease in mobile phase velocity that creates band broadening via longitudinal diffusion. The nonuniformity of the stationary phase, combined with difficulties controlling the atmospheres of the large development chambers, also contributes to difficulties in reproducibility.

The research contained herein seeks to circumvent some of these problems using pillar array systems. Not only do these systems exhibit much greater uniformity, as will be shown, but they also do not exhibit the great decrease in mobile phase velocity with increasing solvent front distance like in TLC. Thus, per the van-Deemter equation, we can decrease our plate height by decreasing our pillar size—or, more accurately, our inter-pillar gap size—without having to sacrifice mobile phase velocity (and thereby increasing longitudinal diffusion). Furthermore, when taken into the nanoscale regime, these systems exhibit fluorescence-enhancement properties that can greatly increase their applicability.

Chapter 2

Introduction to Pillar Arrays

2.1 – History and Basic Principle

Microfabrication methods that were developed for use in the semiconductor industry have been adapted to develop micro- and nano-structured on-chip media with a wide range of possible applications.[21] Notably, they have been used to create microstructures that can not only function as an alternative to the traditional stationary phases used in liquid chromatography columns, but also can be used to create open or pressure-driven planar chromatography systems.[23–31] Silicon wafer technology has often been employed because it allows for creation of features down to the nanoscale, and also because it allows for exact control of the layout and nature of those features.

The work in this research focuses on the creation of pillar arrays by lithography and by thermal dewetting in order to create planar platforms for chromatography and detection. Work previously done by Taylor et al established that pressure-driven pillar array systems could be used for chromatographic separations that exhibited more efficiency than traditional packed bed liquid chromatography columns.[32] Moreover, Kirchner et al found that pillar arrays in both the micro- and nanoscales could be used for open-platform planar chromatography.[15,21] Still others investigated the fluorescence properties of pillar arrays, concluding that nanopillars exhibit optical resonance and field enhancement on their surfaces.[33]

2.2 – Efficiency, or Why to Use Pillars Instead of Thin Layer Chromatography

As stated previously, chromatographic efficiency is known to improve as the particle size of a stationary phase decreases. However, reducing the particle size in traditional systems generally exacerbates nonuniformity in the packing material and increases pressure demands. By contrast, lithographically-created pillar arrays systems are by nature highly ordered and experience less resistance to flow than comparable packed or monolithic columns.[7,34,35] Due to

this, the reduction in mobile phase velocity with decreasing particle size often observed in TLC is less.[9,12] Additionally, these highly ordered pillar arrays have been shown to exhibit negligible eddy diffusion effects, eliminating that source of band broadening.[29,30,32] As a result, even open-platform pillar array systems have demonstrated improved plate height.[21,36]

2.3 – Design of Deterministic Pillars by Photolithography

Photolithography is a lithographic process which takes advantage of polymers known as photoresists which become soluble or insoluble when exposed to light. Advantages of this method include its relative ease, rapidity, and economical nature when compared with other lithographic processes like electron beam lithography. However, it is limited by its scale; the resolution of photolithography is fundamentally restricted by the wavelength of light used and complications due to diffraction.[37]

In a typical photolithographic process, the substrate, often a silicon wafer, is first prepared by cleaning and dehydrating the surface. A photoresist is then applied by spin coating at a predetermined rate to obtain the desired resist thickness. The photoresist may either be positive (polymer become soluble when exposed to light) or negative (becomes insoluble when exposed to light). The wafer is then soft-baked to improve the resist's adhesion to the wafer surface.

Next, the wafer is exposed to light through a mask which has been previously laser written and developed with the desired pattern. Exposure can be performed in one of three methods: contact, projection, or proximity. Contact exposure physically places the mask and the wafer substrate in contact with one another, which offers superior resolution but has the drawback of the potential for substrate damage that causes feature imperfections. Proximity exposure puts a small distance between the mask and substrate, and as a result suffers greatly in

resolution. Projection exposure uses a dual lens optic system to project the image of the mask onto the substrate, and exhibits middle-of-the-road resolution compared to the other two methods.

After the wafer has been exposed, it is baked again. This process, known as post-exposure baking, is of utmost importance to reduce the effect of the incident light hitting the substrate at different angles. When this occurs, the light can travel through the resist and reflect off the wafer surface, creating an interference pattern that will reduce feature quality.[38] Finally, the wafer may be developed in an appropriate solvent to remove the solubilized areas.

The micro-scale pillar arrays developed for this work modified this process slightly in two ways. First, a dual-layer positive photoresist system was used to improve resolution. The bottom layer of photoresist was more sensitive to light than the top layer, creating an undercut when exposed. This assisted with the second modification, which was creation of a hard mask by the physical vapor deposition of chromium. The undercutting caused by the dual photoresist allowed for chromium deposition that exactly matched the feature size of the mask. Without this undercutting, the chromium would not deposit on a large enough area, and the resulting features once etched would be undersized. After development of the resist, a dual electron beam evaporator was used to deposit chromium on the wafer surface. Following this, a lift-off process was performed, removing the photoresist and any excess chromium and leaving behind only the chromium that was deposited directly onto the wafer surface. Figure 2.3.1 illustrates the photolithographic method used in this body of work.

2.4 – Design of Deterministic Pillars by Electron Beam Lithography

In many ways, electron beam lithography (EBL) resembles photolithography. However, because it uses electrons instead of UV light to expose the resist, the size limitations of the

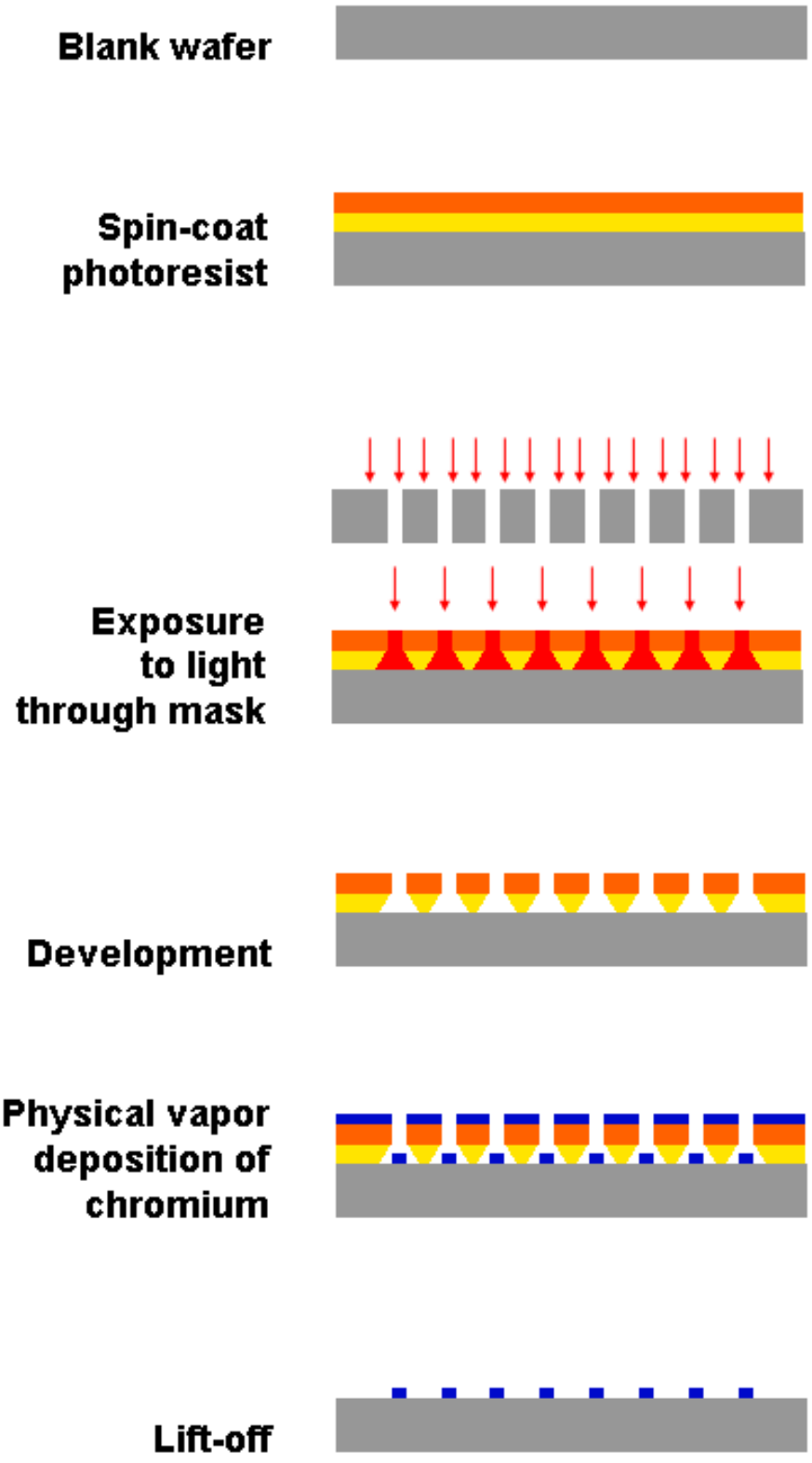

Figure 2.3.1: Illustration of the photolithographic process used in this work

patterns are much smaller. Indeed, if feature sizes smaller than 1 μm are desired, EBL is necessary. This benefit does come at a cost—namely, the directed electrons can only be used to write the pattern serially, and the entire wafer cannot be exposed at once. As a result, the time required to pattern a wafer via EBL is much greater than that required to pattern via photolithography. While the exposure process in photolithography can take as little as several seconds, it is not uncommon for EBL patterning to require days.

A typical EBL system is comprised of an electron gun and a focusing column, all under vacuum. The electrons are generated in the gun using electron emitters or cathodes and then accelerated by an electrostatic field. Electric and magnetic lenses in the column then focus and direct the beam according to a programmed Computer Assisted Design (CAD). The patterning is very sensitive to the energy of the electrons produced. Electrons of too high an energy will result in bleeding and loss of resolution due to overexposure, while electrons of too low an energy will inadequately penetrate the photoresist, causing resolution loss due to inhomogeneity in the developed areas. Due to this, it is of great importance to perform dosage studies when developing a method to ensure that features are patterned as desired. Choice of photoresist and development solvent can similarly affect resolution, and therefore must also be optimized.

Within this work, nano-sized pillars served a significantly different purpose than photolithographically-created pillars. Previous studies have shown that pillars at or near 100 nm in diameter can exhibit a tuneable fluorescence-enhancing field.[33,39] This effect has been used for the detection of surface-immobilized beryllium.[40] Here, it is used for the detections of uranyl and of DNA.

2.5 – Design of Stochastic Pillars

If high order and precise control of the array pattern is not critical, then another method may be used to create nanoscale pillars without the great cost and throughput limitations of EBL. In a process known as dewetting, a thin layer of platinum is deposited onto a p-type silicon wafer on which 100 nm of silicon oxide has been thermally grown. The wafer is then annealed in a 10:1 mixture of Ar:H_2 for a designated period of time at a temperature of approximately 900 °C.[41] During this anneal period, the platinum forms into islands on the wafer surface which can then act as a hard mask for etching, much like the chromium does in photolithography and EBL. These islands are nonuniform, and the position and sizes of the pillars resulting from this process can only be partially controlled. Specifically, by varying the thickness of the platinum film deposited and the anneal time, the average pillar size and spacing may be tuned.

2.6 – Reactive Ion Etching

Once the chromium—or platinum, in the case of the stochastic arrays—hard mask has been created, the wafer is ready to be etched. The etching method used herein was inductively coupled plasma (ICP) reactive ion etching (RIE). ICP RIE is a dry-etch method, meaning the surface is bombarded with chemically active ions instead of using solvents to etch the surface. The ions in this case are produced by a strong radio frequency (RF)-generated magnetic field which strips the ions from the desired gas mixture inside the chamber. The positive gas ions then impact the wafer and react chemically with the surface, although some material removal does occur via sputtering. Figure 2.6.1 illustrates a general RIE chamber. Due to the mostly-vertical delivery of the ions, ICP RIE tends to be anisotropic in nature—that is, the vertical etch rate is greater than the horizontal etch rate.

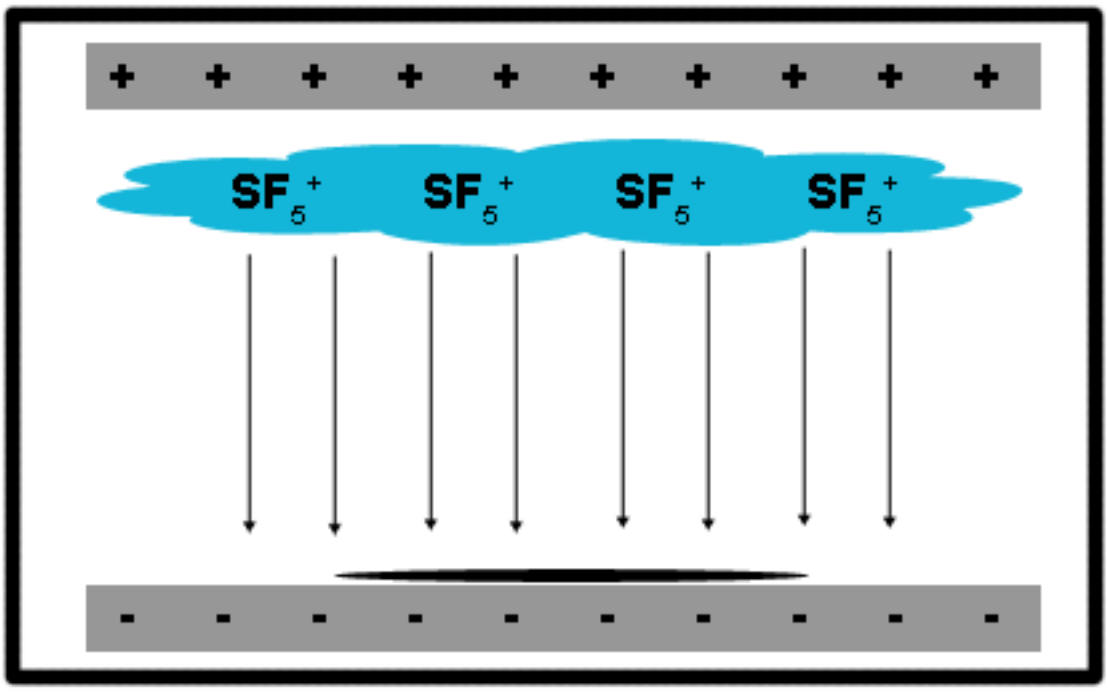

Figure 2.6.1: Schematic of an RIE chamber using SF_5 for etching.

This anisotropic nature is useful when creating high-aspect ratio pillars such as the photolithographically created pillar arrays in this work. Deep reactive ion etching (DRIE) processes such as the Bosch recipe take advantage of time-multiplexed etch and passivation steps.[42] In the etch step, the wafer is exposed to SF_6 gas, which etches silicon isotropically. In the following passivation step, a C_4F_8 polymer is deposited onto the surface. When the cycle repeats, the SF_6 will preferentially etch through the fluoropolymer at the wafer floor—because the ions primarily move vertically—and not through the pillar sidewalls. The cycle may be repeated as many times as necessary to reach the desired pillar height, although excessively long etch times may still result in undercutting as the fluoropolymer begins to have difficulty reaching down in between the pillars. In addition to improving pillar stability and allowing for higher-aspect ratio pillars, this process also allows for better control of pillar height and enhances pillar surface area due to the characteristically scalloped pillar sidewalls it creates. Figure 2.6.2 describes the Bosch process and includes an example of Bosch-etched pillars.

2.7 – Surface Modification

The usefulness of pillar array systems as separation media is mitigated by their limited surface area. Increasing the surface area of a stationary phase increases the retention of an analyte on the system by providing more sites for sorption without needing to resort to a thicker phase.[43] There have been several attempts to increase the surface area of pillar platforms, including by electrochemical anodization, anisotropic etching, applying carbon nanotubes, and using sol-gel techniques.[27] In this work, two differing methods are used, both utilizing plasma-enhanced chemical vapor deposition (PECVD).

In PECVD, deposition of the thin film is achieved after introducing the desired gas between parallel electrodes. Much like in RIE, the gas then becomes a plasma due to excitation

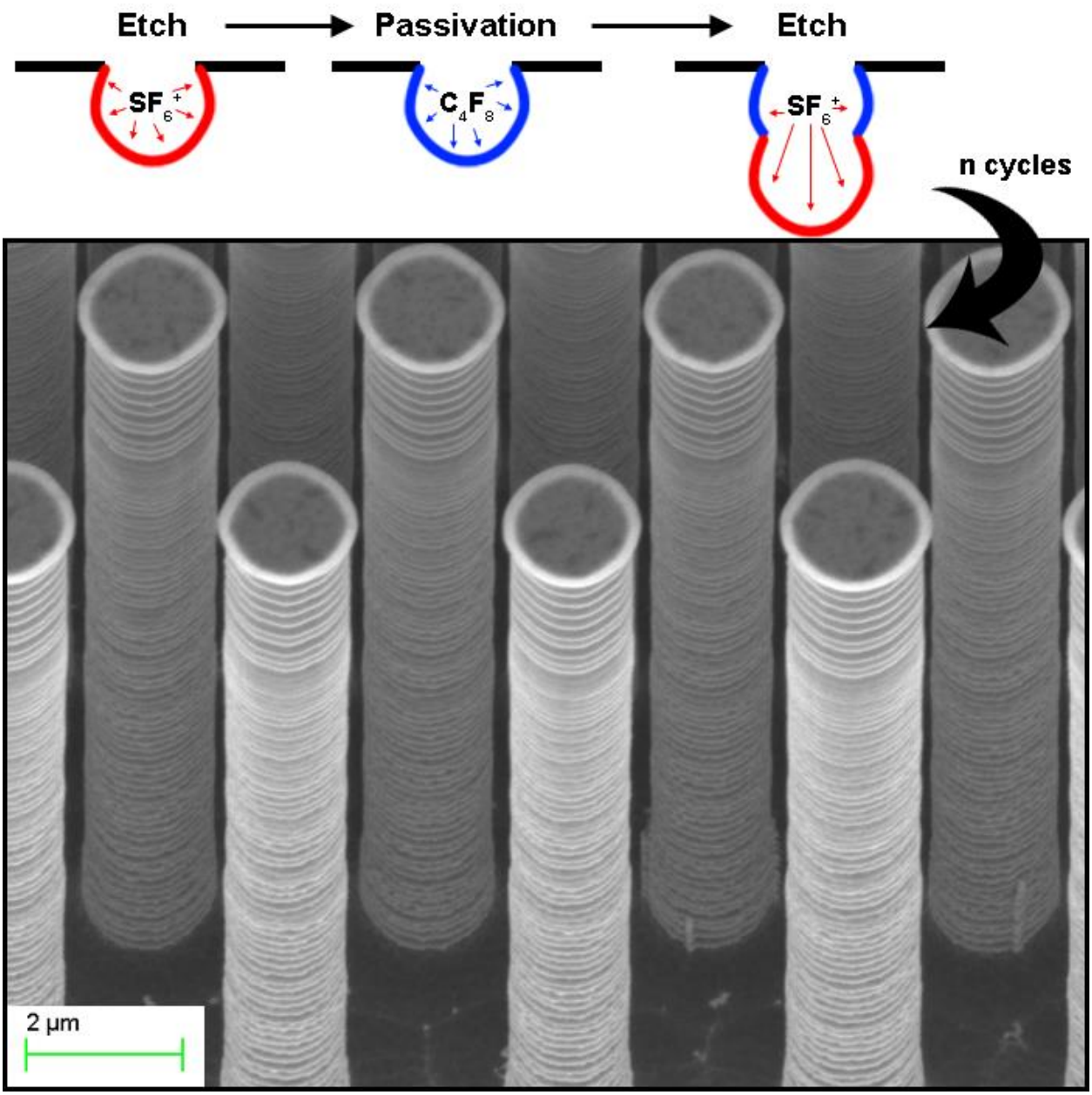

Figure 2.6.2: At the top is an illustration of the Bosch process, which when repeated can produce pillars such as shown at the bottom, with high aspect ratios and characteristic scalloped sidewalls.

by the electrodes. Within the plasma, the introduced gases react with one another, with the reaction products being deposited on the wafer surface. Unlike traditional chemical vapor deposition, this process may be done at low temperatures, from room temperature to a few hundred degrees celcius, which is beneficial when fragile substrates are concerned.

For this research, PECVD was first used to deposit petal-like carbon (PLC), a carbonaceous stationary phase similar to porous graphitic carbon (PGC), which has been used as an alternative to silica-based stationary phases due to its high stability and unique retention mechanisms. Also used was the more typical silicon dioxide, although it was quickly usurped by a method found in the literature for the room-temperature deposition of porous silicon oxide (PSO), which exhibited superior surface area.[44]

In addition to its benefit of high surface area, however, PSO also offered potential benefit as a fluorescence enhancer. Notably, not only does fluorescence scale with surface area, as it allows for increased sample concentrations within the same area, but it also is increased by the highly reflective nature of silicon dioxide.[45]

2.8 – Conclusions About Pillar Arrays

Using technology developed by the semiconductor industry, pillars of different sizes and specifications may be fabricated. While photolithography may be used to create pillars in the micro regime, electron beam lithography or platinum dewetting must be used to fabricate pillars on the nano scale. In this work, photolithographically created pillars were used for chromatography purposes. These pillars were coated using PECVD with either PLC or PSO, both with the intent of increasing the surface area for better retention capabilities. EBL and stochastic pillars, on the other hand, were used for fluorescence-enhancement purposes. These arrays were coated with PSO to sequester our analytes via different functionalizations.

Chapter 3

Capillary Driven Transport in Hierarchically Porous Phases Formed by Conformal Deposition of Petal Like Carbon on Silicon Pillar Arrays

3.1 – Abstract

Surface immobilized porous phases are associated with a variety of capillary phenomena, such as anomalous physisorption, capillary condensation, and capillary-driven flows. Capillary flow is of particular interest as it influences a great many mechanisms in biological and engineered systems. Our group has previously done work exploring separations in lithographically fabricated pillar array systems which use capillary flow as their primary mechanism.[21] The work described here is a logical extension of this previous work, aiming to deposit new on-chip porous-phases with hierarchical porosity. These phases are created using plasma-enhanced vapor deposition (PECVD) of petal-like carbon (PLC). The distinctive nanoscale morphology of PLC is associated with high surface area, which is known to be a prerequisite for high performance stationary phases in analytical systems with high immunity to sample overloading. In addition, PLC, like other porous carbonaceous phases before it, may exhibit unique reversed-phase properties that allow it to be used as a retentive stationary phase without further surface modification. We investigated the functionalities of PLC, including its solvent flow characteristics and porosity. Also examined were its retentive capabilities as a stationary phase for our pillar array systems, as not only did we expect its high surface area increase the efficiency of our separations, but its unique retention mechanisms were hypothesized to allow for the separation of polar analytes.

3.2 – Introduction to Carbonaceous Stationary Phases

Porous graphitic carbon (PGC) is a packing material used in high-performance liquid chromatography (HPLC) columns as a reversed-phase stationary phase.[46–48] It was developed as an alternative to silica-based stationary phases, which contain residual polar silanol groups and have poor stability at extremes of pH and temperature. PGC consists of a conducting planar

surface of intertwined graphitic ribbons. The carbon atoms are connected through covalent bonds into a hexagonal arrangement and the sheets are held together by van der Waals interactions, although successive layers are not oriented regularly.[48] The intertwined nature of PGC lends itself to high rigidity and mechanical stability. It is stable under pH conditions from 0 to 14 and temperatures up to 200°C.[48]

Compared to silica-based RP stationary phases, PGC was prepared with the idea that it would be more hydrophobic as it is constituted of pure carbon and does not contain the residual polar silanol groups mentioned above.[48] However, in addition to hydrophobic interactions, PGC has retention mechanisms based upon the planarity of its surface and the presence of delocalized π-electrons. PGC has been shown to be sensitive to the number of contact points or total contact area between solutes and the surface, with retention preference towards flat aromatic molecules.[48,49] Meanwhile, the presence of delocalized π-electrons at the PGC surface allows for donor-acceptor charge transfer interactions between the lone pair electrons of a solute and the PGC.[50–52] As such, PGC retains not only nonpolar molecules based on hydrophobic interactions, but also can be used to retain polar molecules, so long as the polar group on the molecule is sufficiently available for interaction.[48]

Petal-like carbon is a new derivative of PGC created using a simpler method analogous to the already established method for the deposition of silicon dioxide by PECVD. As such, it is used in this work to not only explore its surface-area increasing capabilities, but also as an alternative to a silicon-based stationary phase with novel retention mechanisms.

3.3 – Fabrication and Deposition of Petal Like Carbon

Planar open-format pillar arrays were generated using a modified version of a technique that generates high-aspect ratio pillar arrays for pressurized systems.[21] All processes were

performed using standard cleanroom lithographic processing techniques at Oakridge National Laboratory (ORNL). Silicon wafers (Czochralski grown, p-type, 100 mm, 300-500 μm thickness, 0.01-20Ω resistivity) were chosen as the base for the arrays. Fourteen chips were arrayed per wafer using Computer Assisted Design (CAD) software defining the pillars as rhomboids laid out in equilateral triangles. The arrays varied in size from 3 cm x 0.2 cm to 3 cm x 3 cm.

A Quintel Inc. contact aligner was used for photolithographic patterning along with a double-layer resist system (lift-off resist LOR-1A overcoated by positive tone photoresist 955CM-2.1, MicroChem Corp.). Following development, chromium (15-20 nm) was deposited onto the wafer with an electron beam physical vapor deposition evaporator. The remaining photoresist was then lifted off the wafer with acetone, taking any excess chromium with it such that only areas which had holes now contained chromium. The chromium then acted as a hard mask during a Bosch process that alternates etching with a passivation layer of fluoropolymer. This anisotropic deep reactive ion etching (DRIE, System 100 Plasma Etcher, Oxford Instruments) was used to form pillars that were 15-20 μm in height.

Following etching, pillars were coated with a thin layer of petal-like carbon (~300 nm) via plasma-enhanced vapor deposition with acetylene and ammonia. Due to the later-discovered fluorescence-quenching nature of PLC, the pillars used for retention studies then received an additional layer consisting of traditional silicon dioxide (~10-20 nm), also via plasma enhanced vapor deposition. Figure 3.3.1 depicts pillars before PLC, after PLC, and after overcoating with SiO_2.

3.4 – Solvent Transport Studies

Flow studies were performed on PLC arrays in order to study solvent interaction. A vertical chamber (~75 mL volume) was constructed for use in development. A clean array was

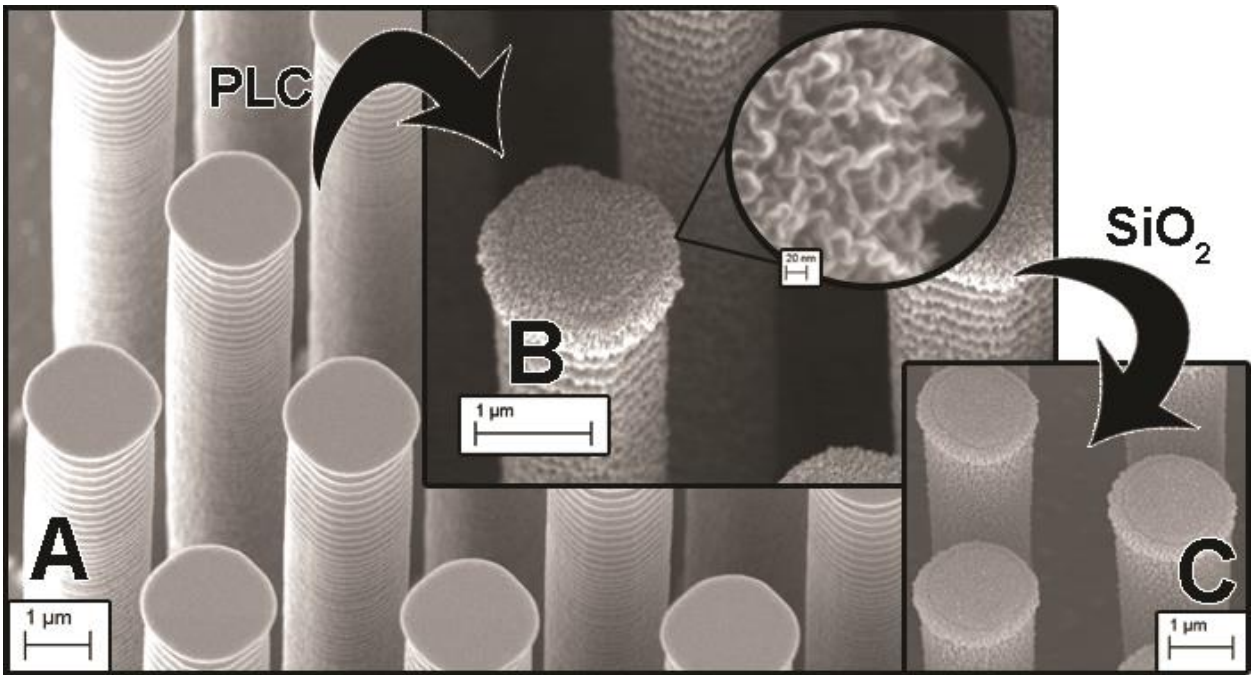

Figure 3.3.1: Photolithographically-fabricated pillars before application of any coating (**A**), after application of PLC (**B**), with inset depicting the characteristic fuzziness of the PLC fibers, and after overcoating with SiO_2 (**C**).

mounted onto a microscope slide and placed within the chamber, which was then closed. Solvent was then pipetted into the bottom of the chamber until the solvent level was just below the array. Once the chamber had come to equilibrium (~1 min), additional solvent was added until the level reached the base of the array. The progress of the solvent front was then monitored using a Playtel^{TM} microscope. This was done with ethanol (EtOH), water (H_2O), N-methyl-2-pyrrolidone (NMP), and mixtures thereof.

Solvent front velocity and uniformity on PLC arrays were compared to those from a traditional octadecyltrichlorosilane (C18)-functionalized array, which was created using a method previously published.[21] According to Guiochon and Siouffi, a linear relationship is expected between the square of the distance the solvent travels and the time it took to travel that distance. This relationship may be described using the equation

$$L^2 = k_0 * t * d_p * \frac{\gamma}{\eta} * \cos\theta \qquad [3.4.1]$$

where L is the distance the solvent front has traveled over t time, k_0 is the bed permeability, d_p is the particle diameter, γ is the surface tension of the mobile phase, η is the viscosity of the mobile phase, and θ is the contact angle the mobile phase exhibits with the stationary phase.[53] Previous work showed that solvent front velocity is mainly determined by the permeability constant of the packed bed and the surface tension to viscosity ratio of the mobile phase.[21] It is notable that a marked deviation from linearity is observed with EtOH on PLC, an effect possibly explained by evaporation of solvent from the array. In support of the hypothesis that the non-linearity of the EtOH curve was due to evaporation, NMP (which has a low vapor pressure) showed no such deviation. Figure 3.4.1 displays the graphs of Equation 3.4.1 with respect to these studies, where it can be seen that PLC exhibited a lower mobile phase velocity than a traditional C18-functionalized pillar array.

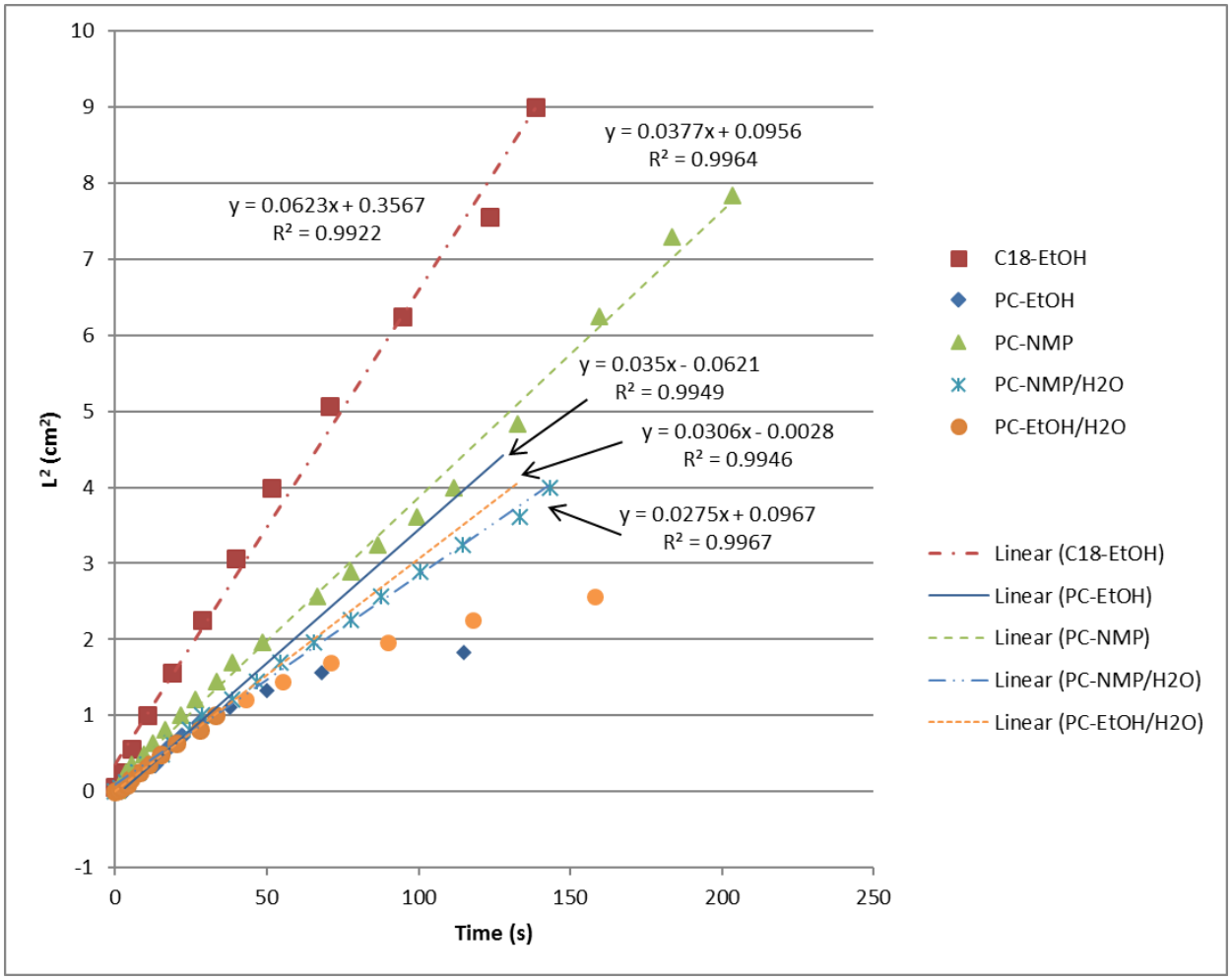

Figure 3.4.1: Relationship of solvent front movement to time for various solvents on a PLC array and a traditional C18 array.

3.5 – Possible Form Change with Increasing Thickness and Preliminary Surface Area Calculations

A small sample (5.1 mg) of PLC was obtained by scraping the coating off several wafers which had undergone the coating process. Brunauer-Emmett-Teller (BET) analysis of the adsorption of N_2 was then used to attempt to determine surface area. This reading reported a surface area of approximately 50 m^2/g, but was near the limit of detection of the BET instrument. The small size of the sample led to a second trial with a greater amount (76 mg). The greater amount was obtained by increasing the deposition time, but it was hypothesized that increasing the deposition time created a change in morphology from more filamentous to something more columnar. This seemed to have affected the porosity of the PLC, as the second BET result returned a surface area of zero.

3.6 – Preliminary Solute Transport Using a Two-Phase System

In the process of investigating the ability of PLC to retain and separate analytes, it was discovered that the carbon—due to its large number of unbound π-electrons—quenches the fluorescence of a wide variety of dyes. As previous work with similar systems have used fluorescence microscopy to do the majority of the visualization of spots and spot movement, this is an undesirable trait.

As a possible solution, we coated PLC arrays with a thin (10 nm) layer of SiO_2, which could then be functionalized with traditional C18 chemistry. Ideally, such a process would provide enough distance between the analyte and the carbon so that fluorescence would not be quenched, without filling in too much of the trademark fibrousness of the phase. Although it did not allow us to observe the unique retention mechanisms of the PLC, this method did allow us to visualize our analytes.

Square 3 cm x 3 cm arrays were created with the majority consisting of functionalized, SiO_2-coated PLC and a thin strip with just plain PLC. However, it was discovered that mobile phase flow was greatly affected across the boundary between non-coated and coated PLC, rendering the two-phase system unuseable. Instead, preliminary solute transport experiments were performed only within the coated PLC. Sulforhodamine (1×10^{-4} M) and coumarin (1×10^{-4} M) were spotted and developed in two dimensions with isopropanol. The system exhibited only modest retention, but some promise for separation. This is shown in Figure 3.6.1.

3.7 – Conclusions About Petal Like Carbon

Although PLC showed promise as a stationary phase, several of its properties make it unsuitable for these pillar array systems in their current incarnation. The fluorescence-quenching nature of the carbon made imaging of spots and developments impossible, and subsequent coating of the phase with silicon dioxide defeats the purpose of investigating its unique retention mechanisms, although it did show some separation capabilities. Furthermore, our inability to properly measure the surface area of the phase, and the possibility of its change in nature with thicker depositions make it unideal for its purpose of increasing the surface area of our pillars.

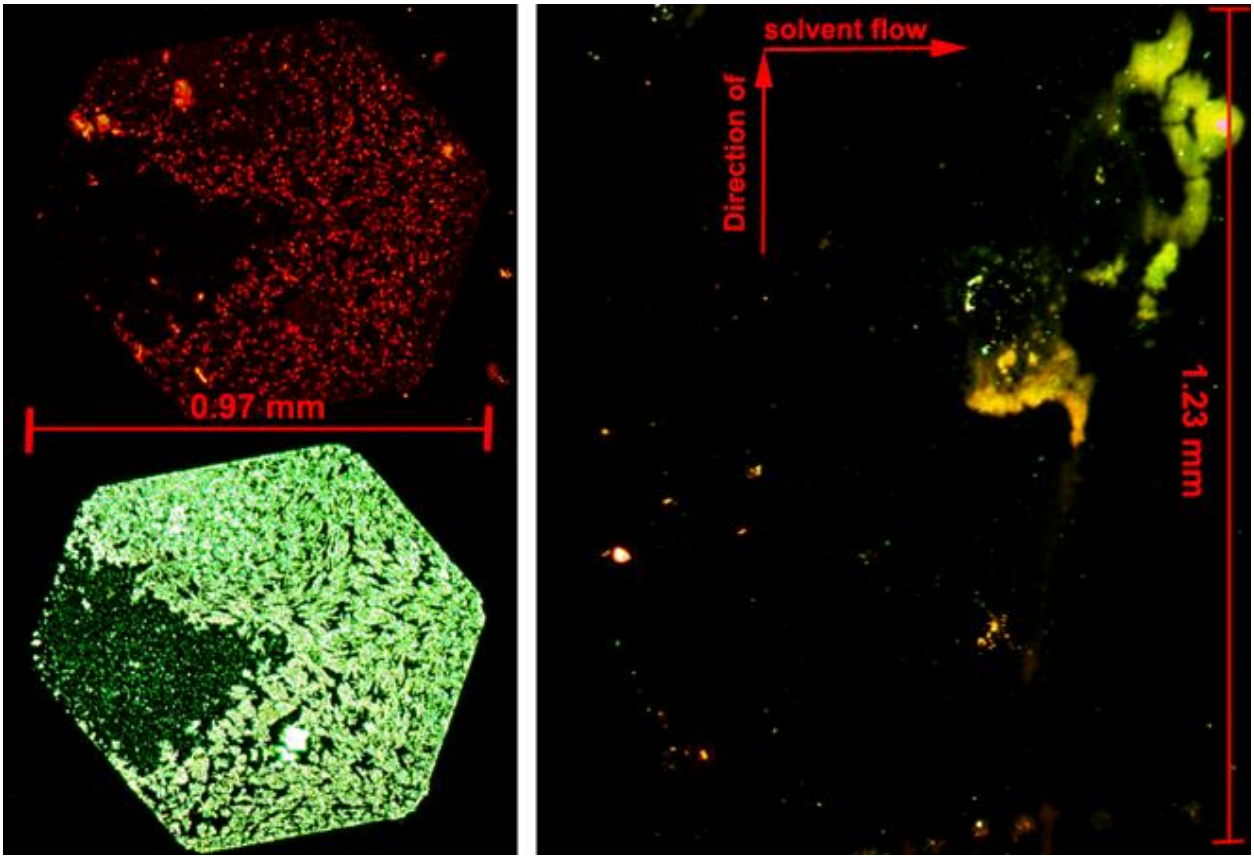

Figure 3.6.1: Coumarin (green) and sulforhodamine (red) pre- and post-development on a SiO_2-coated PLC array with 100% isopropanol. The initial spot, shown on the left, was imaged under green (top) and blue (bottom) excitation to visualize the sulforhodamine and coumarin, respectively. On the developed array, sulforhodamine was visible below and to the left of the coumarin, indicating that it was less retained.

Chapter 4

Retention in Porous Layer Pillar Array Planar Separation Systems

Retention in Porous Layer Pillar Array Planar Separation Platforms

Danielle R. Lincoln, Nickolay V. Lavrik, Ivan I. Kravchenko, and Michael J. Sepaniak

Analytical Chemistry **2016** *88* (17), 8741-8748

DOI: 10.1021/acs.analchem.6b02079

4.1 – Abstract

This work presents the retention capabilities and surface area enhancement of highly ordered, high-aspect ratio, open-platform, 2-D pillar arrays when coated with a thin layer of porous silicon oxide (PSO). Photolithographically-prepared pillar arrays were coated with 50-250 nm of PSO via plasma enhanced chemical vapor deposition and then functionalized with either octadecyltrichlorosilane or n-butyldimethylchlorosilane. Theoretical calculations indicate that a 50 nm layer of PSO increases the surface area of a pillar nearly 120-fold. Retention capabilities were tested by observing capillary action-driven development under various conditions, as well as by running one-dimensional separations on varying thicknesses of PSO. Increasing the thickness of PSO on an array clearly resulted in greater retention of the analyte(s) in question in both experiments. In culmination, a two-dimensional separation of fluorescently derivatized-amines was performed to further demonstrate the capabilities of these fabricated platforms.

4.2 – Introduction

Micro- and nano-scale on-chip separation media have been developed by modifying fabrication processes first used by the semiconductor industry.[23] These techniques have been shown to improve efficiency by replacing the relatively polydisperse and heterogeneous packing particles in traditional packed and monolithic columns with lithographically fabricated high-aspect ratio pillars.[24] Not only has the fabrication of these pillar arrays been successfully replicated, but their advantages as a separation media have been well documented.[7,21,24,25,28,54–56] Efficiency related to mass transfer is known to improve as the particle size of a separation medium decreases, but scaling down traditional systems generally exacerbates nonuniformity in the packing material and its beds, in addition to increasing pressure demands. However, recent

studies have established that nearly perfect pillar arrays exhibit less resistance to flow than comparable packed and monolithic columns, and combined with their high order these arrays should exhibit an improvement over traditional media.[7] Indeed, our group's previous work with pillar arrays for ultra-thin layer chromatography (UTLC) has demonstrated improved plate height (H).[21] Moreover, non-lithographically created pillar arrays, such as the UTLC arrays created by Linford *et al* by depositing silicon nitride onto carbon nanotube templates, or the glancing angle deposition UTLC plates created by Brett *et al*, have been shown to be valuable advances to separation chemistry.[10,57,58]

Perhaps one of the most promising applications of pillar UTLC is its ability to be used as a two-dimensional separation platform. Pillar arrays have the potential to meet all three of the criteria for a true 2-D separation, because it is possible to develop in two dimensions with different mobile phases without having to transfer analytes from one medium to another.

Overall, however, the usefulness of pillar arrays as separation media is mitigated by a limited surface area. It is well established that increasing the surface area of a stationary phase increases the retention of analyte in the system by providing more sites for sorption while simultaneously maintaining a thin sorbent layer.[43] Desmet *et al* demonstrated that porous silicon can be used to increase surface area in pressurized and confined ordered systems, while Olesik *et al* used a mat of spun polyacrylonitrile to generate a porous layer and create an open UTLC platform.[12,27,54,59,60] Previous research from our group has shown that highly ordered micro-pillar arrays, coated with a thin layer of silicon oxide and functionalized with a hydrocarbon reversed stationary phase, can produce plate heights of less than 1 μm in closed pressure-driven systems and plate heights on average of 2 μm in open, capillary-action-driven array systems.[25,29,54,61–63] Studies have found that room temperature plasma enhanced chemical vapor deposition (PECVD)

of silicon oxide creates a thin, conformal porous silicon oxide (PSO) layer.[44,64] Crane *et al* were able to use PSO to investigate closing the gap between pillars and its effect on solvent flow and efficiency.[20] In this work we examine the effect of applying PSO to UTLC systems for the purposes of investigating its effect on analyte retention. The retentiveness and band dispersion of varying thicknesses of PSO is examined, along with the effect of solvent polarity on analyte retention. After these preliminary studies, the effectiveness of the system as both a 1-D and a 2-D separation platform is evaluated.

4.3 – Experimental

Fabrication

Figure 4.3.1 depicts the overarching steps in the fabrication process. First, high aspect-ratio pillar arrays were designed using CAD software defining the pillars as rhomboids laid out in equilateral triangles. Silicon wafers (Czochralski grown, p-type, 100 mm, 300-500 μm thickness, 0.01-20Ω resistivity) were chosen as the base of the arrays, with the arrays being 3 cm x 3 cm. After deposition of a double-layer resist system (lift-off resist LOR-1A overcoated by positive tone photoresist 955CM-2.1, Microchem Corp.), a Quintel Inc. contact aligner was used for photolithographic patterning. The contact aligner exposes the wafer to UV light through a mask, such that after development there are holes in the photoresist where the pillars will be. Chromium (15-20 nm) was then deposited onto the wafer with an electron beam physical vapor deposition evaporator. The remaining photoresist is then lifted off the wafer, taking any excess Cr with it such that only areas which had holes now have Cr. The Cr then acts as a hard mask during a Bosch process that alternates etching with a passivation layer of fluoropolymer. This anisotropic deep reactive ion etching (DRIE, System 100 Plasma Etcher, Oxford Instruments) was used to form pillars that are 15-20 μm in height. The resulting pillars also had a mean

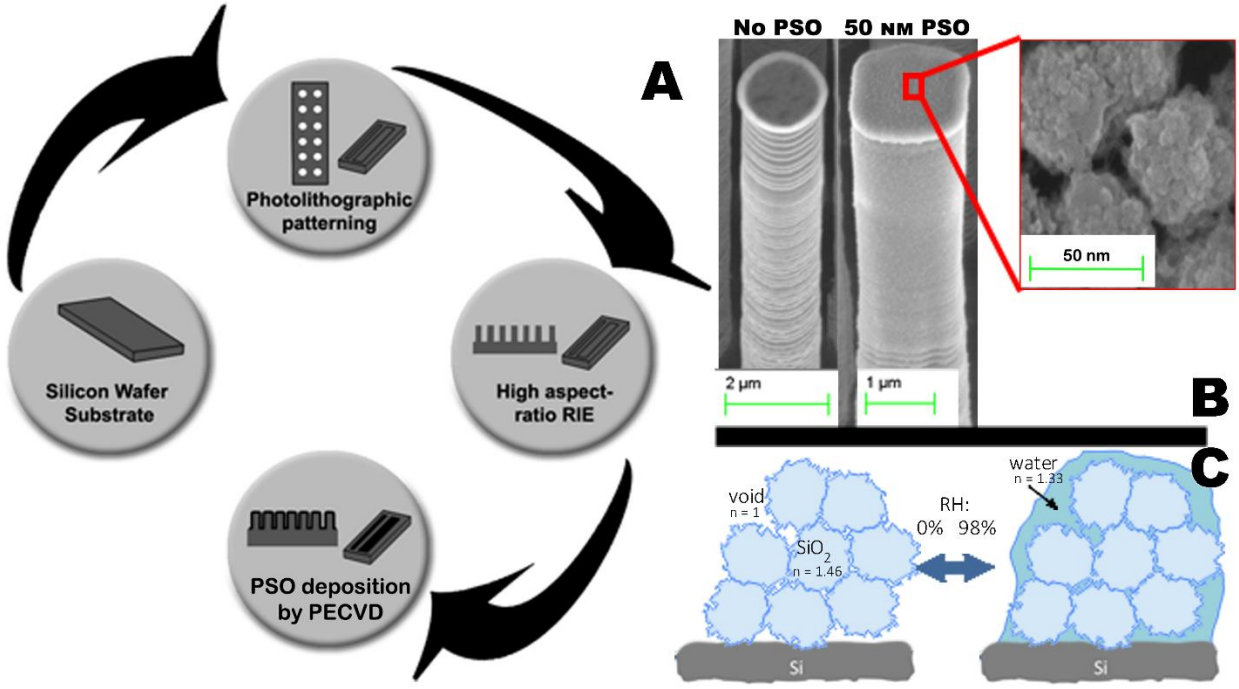

Figure 4.3.1: **A** pictorializes the fabrication sequence, which begins with a silicon wafer substrate that is photolithographically patterned. The wafer is then etched with anisotropic DRIE and coated with a thin layer of PSO via PECVD. **B** shows an SEM of a pillar before and after deposition of 50 nm PSO, with a close-up of the PSO granules included. **C** describes the three-component effective medium model used to determine void fraction in PSO, composed of SiO_2, void, and H_2O.

diameter of 2 μm and a mean pillar gap of 1.5 μm. Although the previous work by Crane *et al*[20] showed the advantage of decreasing pillar and pillar gap size, slightly greater gap sizes were chosen so that greater thicknesses of PSO could be deposited without closing the inter-pillar gap.

Following etching, pillars were coated with a thin layer of porous silicon oxide (2, 4, or 6 minute deposition time) via room temperature plasma-enhanced chemical vapor deposition (PECVD, System 100 Plasma Deposition Tool, Oxford Instruments).[21] Unlike wet chemistry methods of creating a porous silicon oxide layer, this method coats the surface of the pillar arrays instead of etching into them. This retains the integrity of the pillars and requires no post-annealing process. In addition to increasing the surface area of the arrays, the PSO is rich in free silanols, allowing for functionalization of the arrays with either octadecyltrichlorosilane (C18) or n-butyldimethylchlorosilane (C4) and making it a suitable substrate for reversed phase chromatography.

Functionalization

Functionalization with C18 has been described previously.[21] The pillar array was first treated with equal parts nitric and sulfuric acids for 30 minutes, followed by drying at 120 °C overnight. The array was then submerged in 10% octadecyltrichlorosilane in toluene (to minimize polymerization) and heated to 170 °C for 2 hours. Then the array was rinsed in toluene, tetrahydrafuran, 90/10 tetrahydrafuran/distilled water, and distilled water, each rinse lasting 10 minutes and repeated once before moving on to the next rinse. In the C4 functionalization, the arrays were first treated with acid and dried as in the C18 functionalization. Then they were placed into a desiccator overnight with an open dish containing a 10% solution of n-butyldimethylchlorosilane in toluene (to maximize evaporation) before following the same rinse procedure as with the C18 functionalization.

Determination of PSO porosity/surface area

Following fabrication, arrays were imaged using Merlin scanning electron microscopy (SEM) to determine PSO thickness and to visualize the PSO morphology. Figure 4.3.1 shows a typical image of the arrays, with the characteristic pebbled texture of the PSO visible. This morphology was then used to estimate the surface area increase due to the porous layer.

In addition, ellipsometry was used to characterize degree of porosity of PSO deposited onto an unaltered silicon wafer. For ellipsometric measurements, PSO was deposited on silicon substrates using a deposition time of 110 seconds. Ellipsometric data were acquired at the probing wavelength of 633 nm and incident angle of 55 degrees using a Beaglehole spectroscopic imaging ellipsometer (SIE, Beaglehole) equipped with a sample flow cell. The flow cell was fed with a mixture of saturated water vapor and dry nitrogen gas (99.99 purity) and allowed us to acquire ellipsometric angles as a function of relative humidity (RH) in the range of 0-98 % with accuracy of 3%. Humidity was measured by a humidity sensor (Omega engineering USB sensor) at the outlet of the flow cell. These values were used to calculate refractive indices for dry and humid conditions, which were then applied to a three-component effective medium model, as shown in Figure 4.3.1, to determine void fraction.

The surface area factor increase on pillar arrays was determined via fluorescence increase. Array fragments with 0, 50, 100, and 150 nm of PSO were functionalized with 3-aminopropyltriethoxysilane (APTES) by placing the pieces in a 10% v/v APTES/toluene solution and soaking at room temperature for 1 hr. The pieces were then sequentially rinsed with toluene, methanol, and deionized water and then were soaked in 1 mM fluoresceinisothiocyanate (FITC) (in ethanol) for 45 min. After a triplicate rinse in ethanol to remove any excess FITC, fluorescence imaging of the pieces was performed with a Nikon Eclipse E600 microscope and Q-capture software. Multiple ($n \geq 7$) 102 pixel x 102 pixel square areas on the green channel of each

image were then integrated and averaged to obtain the mean gray value. These values were then corrected by subtracting the average mean gray value of an equivalent area without the APTES/FITC treatment. Error was then taken as the standard deviations of the integrations. Comparing the corrected fluorescence values to one another then indicated the surface area factor increase (see Table 4.3.1).

Retention and Efficiency Studies

The retentive capabilities of the arrays were tested by observing analyte development. A chamber for vertical development was constructed from a 20-dram vial. A hole was drilled in the top such that a moveable piston could be inserted into the chamber, and to which the array could be attached so it could be brought into contact with the solvent well below it. Additionally, a sponge was placed in the solvent well against the back of the chamber to facilitate even vapor distribution of the mobile phase. Analyte detection before and after development was obtained via fluorescence imaging with a Nikon Eclipse E600 microscope and Q-capture software. Retention experiments were performed using coumarin 153 (LambdaPhysik, 1 x 10^{-5} M) with varying thicknesses of PSO coating on the arrays (2-, 4-, or 6-minute deposition times), varying mobile phases (ethanol, methanol, or isopropanol, each in varying concentrations in water), and varying functionalization reagent.

Separations

One-dimensional separation experiments were performed with a four-component dye mixture of coumarin 153 (Lambda Physik, 2 x 10^{-5} M), coumarin 2 (TCI, 1 x 10^{-5} M), coumarin 120 (Aldrich, 1 x 10^{-5} M), and sulforhodamine 640 (Exciton, 1 x 10^{-6} M) with varying PSO thickness (2', 4', or 6' deposition time) and varying functionalization method. Separations were carried out in 50% by volume ethanol:water on C4 arrays and a C18 array. One-dimensional

Table 4.3.1: Surface area factor increase due to PSO, determined by fluorescence

PSO thickness (nm)	Corrected mean gray value	Times greater than 0 nm	Times greater than 50 nm
50	2117 ± 441	43	--
100	17153 ± 1612	345	8
150	30248 ± 2935	609	14

development was performed in the same chamber as in the retention experiments. Detection was performed via fluorescence imaging with the Nikon microscope and software described above.

Two-dimensional separation experiments were carried out using a mixture of 7-chlor-4-nitrobenzofurazan-derivitized amines (NBD-amines). A 3 cm x 3 cm pillar array with 150 nm PSO was functionalized with C4. NBD-amines were prepared by mixing 5 mL of a 2.95 M solution of the desired amine (in methanol) with 10 mL of a 0.1 M solution of $NaHCO_3$ (Fischer Scientific, pH 9) and 25 mL of a 0.05% (w/v) solution of 7-chlor-4-nitrobenzofurazan (Acros Organics) in methanol. After 60 min at 55°C, the derivatives were diluted to the desired concentration. A six-component mixture containing NBD-heptylamine (5×10^{-4} M), NBD-hexylamine (5×10^{-4} M), NBD-1-amino-5-hexene (5×10^{-4} M), NBD-pentylamine (5×10^{-4} M), NBD-butylamine (5×10^{-4} M), and NBD-propylamine (5×10^{-4} M) was spotted in the lower left corner of the array. Development in the first dimension was carried out using a 40% by volume ethanol:water solution. Following this, the array was dried and imaged and then the array was rotated and development in the second dimension was carried out with a 40% by volume ethanol:water solution containing 0.038 M $AgNO_3$. Development was performed in a chamber similar to that used for the 1D separation and retention experiments. Detection was again performed via fluorescence imaging with the Nikon microscope and software.

4.4 – Results and Discussion

Characterization of Porous Shell-Core Pillars

It was determined via SEM that the 2-minute deposition of PSO resulted in a layer of 50 nm on the pillar sidewalls, the 4-minute deposition resulted in a layer of 100 nm, and the 6-minute deposition resulted in a layer of 150 nm. Although the deposition of PSO on a flat wafer surface follows a linear relationship with the deposition time (~90 nm/min), the inability of the

plasma to adequately reach between the pillars creates a growth pattern that is slower than anticipated, resulting in a deposition approximately 70% less than predicted for the flat surface. Moreover, while PSO deposited on a flat wafer appears to change morphology as thickness increases from clusters of granules to a more columnar shape, PSO deposited on pillar walls does not appear to undergo this change, likely because of the thin layers deposited.

The ellipsometric angles acquired were fitted at the two extreme values of humidity, RH=0% and RH 98%, to an optical model that consisted of a single-crystal silicon substrate and a film with variable refractive index and thickness. A multi-iteration fitting procedure was performed in DeltaPsi2 software (Horiba), which allowed us to determine geometric thickness (d=144 nm) of the PSO film and its effective refractive indices for dry and humid conditions, n_{RH0}=1.29 and n_{RH98}=1.41, respectively. By applying these values of refractive indices to a three-component effective medium model (composed of SiO_2, void and H_2O) and assuming that nanosized pores in PSO are voids free of water at 0% RH and that they are completely filled with condensed water at 98% RH, we determined that the fraction of voids in dry PSO film was 34%.

Using the porosity estimate and the morphological assumption that the PSO acts as a close-packed arrangement of spheres, we calculated that depositing 50 nm of PSO on a pillar results in a surface area increase by a factor of nearly 120. The method of these calculations is shown in the supplemental information (see Appendix). Similarly, depositing 100 nm results in a factor increase of 240 and depositing 150 nm results in a factor increase of 370.

Using the experiments determining surface area increase by fluorescence, we calculated that depositing 50 nm of PSO resulted in a surface area factor increase of 43, depositing 100 nm of PSO resulted in a surface area factor increase of 345, and depositing 150 nm of PSO resulted in a surface area factor increase of 609. While there is some agreement between the model and

the FITC experiment, there is a discrepancy in the magnitude of the surface area increase. This is possibly because the propensity of APTES to polymerize increases with increasing surface area of the underlying phase, resulting in an artificially inflated area for the FITC to bind to. Additionally, in experiments with 50 nm PSO, we observed a S/N ratio of only 5, and this could have negatively affected our observed surface area factor increase.

Retention Properties

The retentive capabilities of PSO-coated micro-scale pillar arrays was first examined by observing the retention of Coumarin 153 on a C4-functionalized, 50 nm PSO-coated array. There are a number of solvent characterization parameters used in chromatography, such as mobile phase polarity index (P').[29] P' values can vary from less than 0 for fluorochemical solvents to 10.2 for water. Figure 4.4.1 shows the retardation factor, R_f, of the dye versus P' of the various solvents used in this study. P' is computed for mixed aqueous-organic solvents as follows

$$P' = \varphi_{water} P'_{water} + \varphi_{org} P'_{org} \qquad [4.4.1]$$

with P' values taken from tables[63] and φ being volume fraction.

In general, a change of P' by two units is expected to result in a 10-fold change in capacity factor, k', where

$$k' = \frac{1}{R_f} - 1 \qquad [4.4.2]^{65}$$

Our results suggest that a change of P' by two units changes the capacity factor 30-fold, in rough agreement with this expectation, although the overall trend in retardation factor is nonlinear. As polarity increases, the retention of the Coumarin 153 is at first fairly level, but above an index value of 7.5 the retention sharply increases. It was not possible to achieve solvent flow with any mobile phase of higher polarity index than 8.2 as the solvent does not

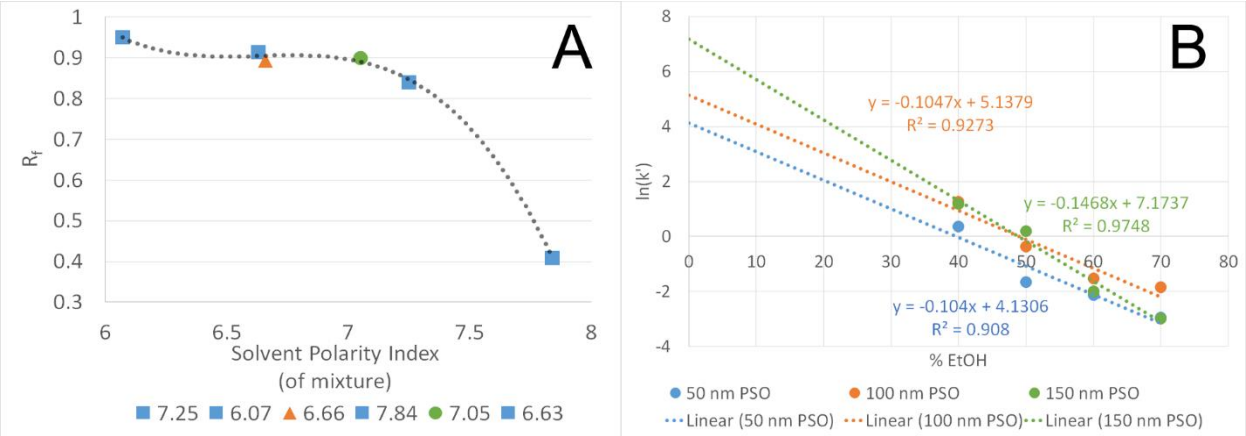

Figure 4.4.1: **A** shows the retention of coumarin 153 versus the solvent polarity index of the mobile phase used. Blue squares indicate ethanol as the organic modifier, the orange triangle indicates methanol, and the green circle indicates isopropanol. **B** shows the ln(k') of coumarin 153 versus the percent of organic modifier (ethanol) for 50 nm PSO, 100 nm PSO, and 150 nm PSO.

adequately wet the hydrophobic surface and wick during development. It is possible that the inability of the mobile phase to adequately wet the stationary phase is accountable for the sharp increase in retention with higher polarity (higher water content) solvent mixtures. Moreover, the open planar chromatography systems at the UTLC scale can be susceptible to evaporation even when care is taken to saturate the vapor above the pillar array.[21] Thus, the composition of the mixed solvent might change as development proceeds and along the development dimension.

Although P' is a common measure of solvent strength, and useful for determining appropriate solvent mixtures, other terms have also been used to evaluate separation systems. One such term, solvent strength (*S*), is related to the strength of the organic modifier in reversed-phase systems, and for a given system, is often observed to be relatively constant.[66] Although *S* remains fairly constant for a given system, it has been shown to vary slightly with different organic modifiers, different solutes, and different reversed phase packings.[67] *S* falls out of the straight line relationship between ln(k') and the fraction of organic modifier according to the equation

$$\ln k' = \ln k'_0 - S\varphi \qquad [4.4.3]$$

where φ is the fraction of organic modifier, in percent, and ln(k'$_0$) is the retention factor of the analyte in pure water, which can be extrapolated from the plot.[66] Desmet *et al* used this relationship to examine their sealed, pressure-driven porous pillar arrays. Their *S* values were comparable, but slightly larger, than typically cited solvent strength value for methanol in a reversed-phase system.[60]

Our system is an open porous pillar array platform similar to TLC, relying on capillary flow to wick the mobile phase, unlike Desmet *et al*, but we still wanted to draw a comparison between the two systems since both dealt with porous silicon pillar arrays. As such, the effect of

increasing the PSO thickness was analyzed by observing the retention of coumarin 153 on C4-functionalized pillar arrays with 50, 100, and 150 nm PSO at varying fraction of organic modifier (ethanol) in the mobile phase. Figure 4.4.1 shows the graph of this relationship, ln(k') vs φ, for the three PSO thicknesses. Although we would expect the slopes for the lines of the three thicknesses to be the same, retention on the 150 nm PSO array developed with 70:30 EtOH:H_2O was consistently less than retention in the 100 nm PSO array. This may be due to unexpected changes in the morphology of the PSO in the thicker phase, as we found occurs on flat substrate (see above).

Our solvent strength values are 100-fold less than Desmet *et al* reported, and 10-fold less than Snyder reported.[60,67] The disparity between *S* values may come in part from differing mobile phase, but more likely comes from the differences in systems, namely that our system is open-platform, and therefore must take into account wicking and evaporation factors. Both Desmet *et al* and Snyder report values based upon closed, pressure-driven systems—Snyder from LC and Desmet *et al* from pillar arrays.

In addition to using it to compare systems, we also used the relationship between ln(k') and φ to examine the surface area increase with different thicknesses of PSO, much like Desmet *et al* used it for their porous-shell pillars.[60] We extrapolated values of $\ln(k'_0)$ for the three PSO thicknesses, and from them calculated k'_0.

By comparing these values, we determined that the effective retentive surface area increases by a factor of ~3 when increasing the PSO thickness from 50 nm to 100 nm, and increases by a factor of ~14 when increasing the PSO thickness from 50 nm to 150 nm. Here there is closer agreement to our geometric model at smaller thicknesses of PSO, but deviations from model behavior at greater thicknesses. By comparison, calculations from our geometric

model predict a factor increase of 2 by increasing the PSO thickness from 50 nm to 100 nm, and a factor increase of 3 when increasing from 50 nm to 150 nm. Calculations from the FITC experiment, on the other hand, indicate a factor increase of 8 when increasing from 50 nm to 100 nm, and a factor increase of 14 when increasing from 50 nm to 150 nm.

Efficiency

Theoretical plate height, H, is influenced by a combination of complex factors generally summarized by the Van Deemter equation,

$$H = A + \frac{B}{\mu} + (C_s + C_m)\mu \qquad [4.4.4]$$

where A represents eddy diffusion, B represents longitudinal diffusion, and C_s and C_m represent resistance to mass transfer in the stationary and mobile phases, respectively. In our systems, we generally ignore eddy diffusion due to the highly ordered nature of our pillar arrays. The aforementioned publication based on anodized porous pillars involved a detailed study of the effect of porous layers on efficiency including the development of an analytical model.[60] Van Deemter plots showed an increase in the resistance to mass transfer at higher flow rates as the porous layer thickness increases. They attribute the increase in C-term to anodization of the floor of pillar arrays, creating a porous layer and non-uniformity.[60]

While we also have a porous floor, our cursory consideration of efficiency herein involves platforms and operations that have considerable differences as well. From a morphological standpoint, our systems have significantly smaller pillar diameters and higher aspect ratios, making it more difficult for PSO to reach deep between the pillars, which may minimize the adverse floor effect. We employ capillary action driven flow which while simple is limiting in terms of attainable and consistent flow rates. The permeability of uniform pillar arrays is greater than for TLC beds of similar feature size. Nonetheless, it is only in the very

early development process that mass transfer is limiting; during most of the development molecular diffusion is contributing mostly to H.[21] The same is true for nanoscale pillar arrays.[15]

To determine whether molecular diffusion and/or resistance to mass transfer in the stationary phase was the primary source of band broadening as PSO layers are added, a cursory evaluation of efficiency was calculated experimentally using the equation

$$H = \frac{\sigma^2}{L} \qquad [4.4.5]$$

where σ represents one-fourth of the apparent spot size after development and L is the distance traveled by the spot. In some cases, the initial spot exhibits a concentrating effect upon solvation by the moving solvent front, a phenomenon previously visualized by Kirchner *et al*.[15]

Due to this phenomenon, the final band size was at times smaller than the initial spot. In order to prevent negative values for H, we assumed an infinitesimally small initial spot. This, in turn, resulted in inflated values for H. Figure 4.4.2 shows the results of these efficiency calculations for the different thicknesses of PSO using different ethanol concentrations in the mobile phase. Although the values themselves are artificially enlarged, the trends depicted are sound. In our system, efficiency decreases (shown by an increase in H) as the thickness of PSO increases. Combined with the observation that thicker stationary phases exhibited faster mobile phase development than thinner phases, this suggests that the C-terms may be significant, although further studies are warranted.

Separations

The chromatographic capability of the system was first demonstrated by separating laser dyes. The four components of the dye mixture were separated in each of the four trials, to varying degrees. The retention of the dyes generally increased with increasing PSO thickness, resulting overall in better resolution. Figure 4.4.3 diagrams the separation results. In addition to

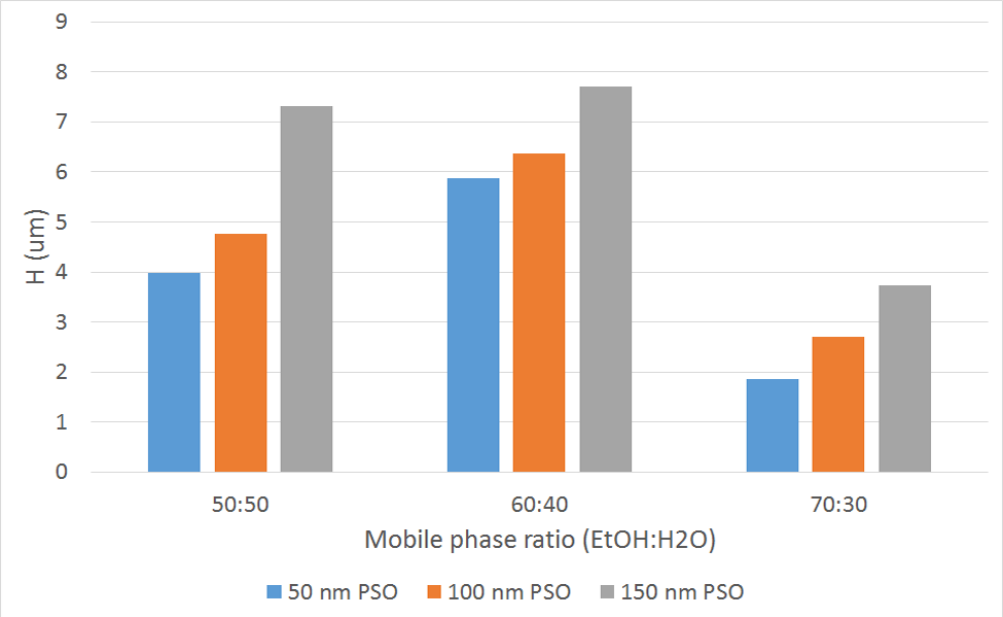

Figure 4.4.2: Cursory evaluation of efficiency trends, given by plate height (H), of the arrays with three different thicknesses of PSO (50 nm, 100 nm, and 150 nm) using Coumarin 152, shown as a function of mobile phase ratio (ethanol:water). Although the individual values are somewhat inflated, the overall trends depicted reflect the decrease in efficiency as PSO thickness is increased.

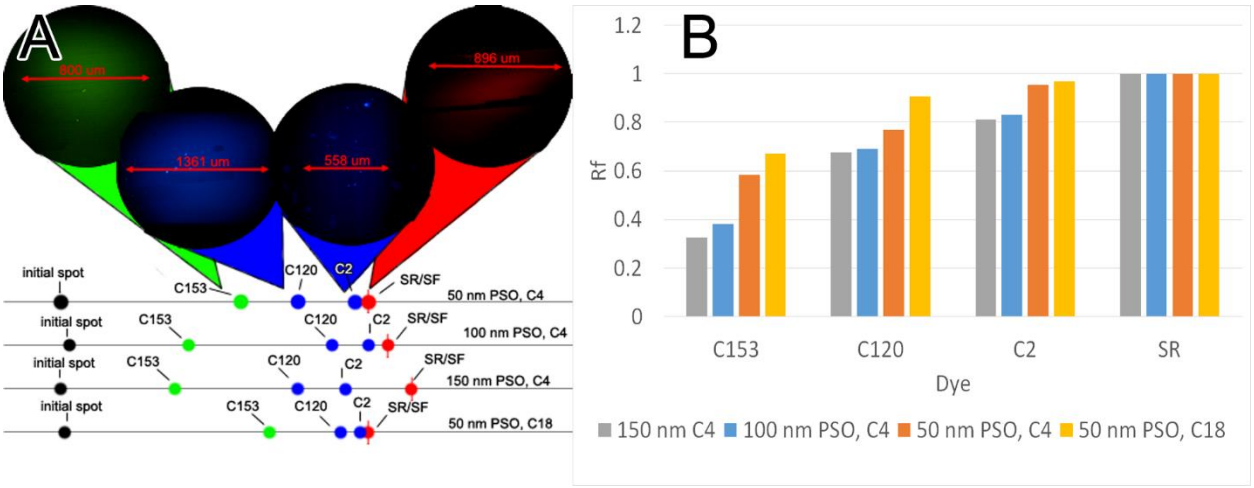

Figure 4.4.3: **A** depicts the spot locations of the dye in the dye mixture, as separated on 4 different arrays (100 nm PSO C4 functionalized, 50 nm C4 functionalized, 150 nm PSO C4 functionalized, and 50 nm PSO C18 functionalized) relative to one another, with the length of the line corresponding to the full 3 cm length of the array. The initial spot location is shown in black, the location of the Coumarin 153 is shown in green, the location of the Coumarins 120 and 2 are shown in blue, and the location of the Sulforhodamine, which is unretained, is shown in red. **B** is a graph of the retardation factors of the different dyes on the different arrays.

the differences occurring as a result of changing the thickness of PSO, there is a significant difference in the separation capabilities between the C4 phase and the C18 phase. Despite C18 having more nonpolar character, C4 exhibited better resolution and retention. If the two phases functionalized equally well, we would expect that C18 would have the greater retention. As a result, it is likely that the gas-phase C4 reaction has a better ability to penetrate PSO pores and produce more complete coverage.

The results of the two-dimensional separation are depicted in Figure 4.4.4. We see in the second dimension separation of analytes which were coretained in the first dimension, although there is a staggered effect due to a lateral vector in the mobile phase flow of the second dimension. In order to be considered a comprehensive 2D separation system, three criteria must be met: transfer from one dimension to the other must result in minimal loss of analyte or degradation of efficiency; the sample components do not recombine during transfer nor during the separation in the second dimension; and the separations in the two dimensions must occur by different mechanisms.[68] Because both dimensions occur on one array with no need for transfer, and the solvent flow in the second dimension occurs perpendicular to the first, our system satisfies the first two conditions. The silver added to our second dimension's mobile phase adds a different mechanism, as silver salts have been shown to form π-complexes with olefins and decrease their retention,[69–73] and when run individually, we observed less retention of NBD-1-amino-5-hexene when using a mobile phase containing $AgNO_3$. Furthermore, in our 2-D separation, we were able to observe the separation of two co-eluted components, NBD-hexylamine and NBD-1-amino-5-hexene, due to this. However, both dimensions separate via reversed-phase chromatography, and so cannot be truly orthogonal. This is supported by the observation of a slightly diagonal pattern in the final positions of the components. Giddings and

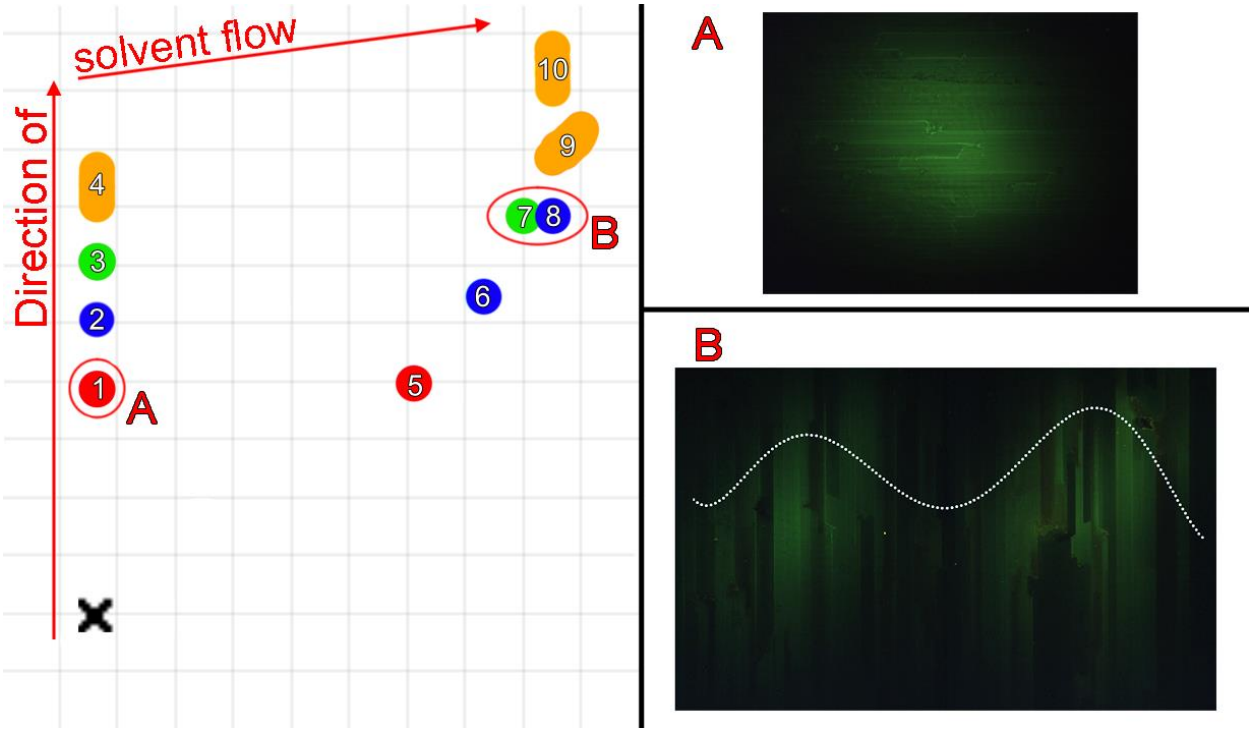

Figure 4.4.4: On the left is a diagram of the NBD-amine locations after development in the first (40:60 EtOH:H_2O) and second (40:60 EtOH:H_2O with 0.038 M $AgNO_3$) dimensions. In the first dimension, in order from most to least retained, are heptylamine (1, red), hexylamine and 1-amino-5-hexene coeluted (2, blue), pentylamine (3, green), and butylamine and propylamine coeluted (4, orange). In the second dimension, the coeluted amines are separated and we see, from most to least retained, heptylamine (5, red), hexylamine (6, blue), pentylamine (7, green), 1-amino-5-hexene (8, blue), butylamine (9, orange), and propylamine (10, orange). There is a staggered effect—most notable for hexylamine and 1-amino-5-hexene—due to a lateral vector in the movement of the mobile phase in the second dimension. **A** shows an image of NBD-heptylamine after development in the first dimension. **B** shows an image of NBD-pentylamine and NBD-1-amino-5-hexene after development in the second dimension, superimposed with the plot profiles of the two spots to show the resolution between the two spots.

Keller explained that a separation that is truly orthogonal will utilize the full separation space present, resulting in a random distribution of sample components.[74]

Despite this, the ability to double the development distance without having to transfer sample from one medium to another is a distinct advantage, as the limited development distance in TLC is one of its more significant drawbacks. Therefore, although our system does not realize its full potential by using all of the available separation space, and therefore does not exhibit the very high peak capacity of a true 2D separation, there is a marked increase in peak capacity to be gained by separating in two dimensions in this way. As described by Giddings, peak capacity of a separation with unit resolution may be calculated using

$$N_c = \frac{L}{4\sigma} \qquad [4.4.6]$$

where L is the distance over which peaks can be distributed and σ is the average standard deviation of the peaks.[22] The peak capacity of a 2D separation is equal to the product of the peak capacities of the 1D methods within it.[68] With an average σ of 640 μm in the first dimension and 750 μm in the second, our system has a potential peak capacity of approximately 53.

4.5 – Conclusion

In this work, we demonstrate that porous silicon oxide can serve as a retentive and high capacity stationary phase modifier for pillar array systems; effectively creating porous shell-core pillar arrays. We showed via three different methods the increase in surface area due to deposition of PSO on the pillars. While there was a slight increase in theoretical plate height with increasing PSO thickness, we did observe an increase in retention. In addition, PSO on 2D pillar arrays allowed us to carry out successful 1-D and 2-D separations, indicating that it does indeed improve the efficacy of pillar array systems. Looking forward, we hope to apply these

findings towards systems of smaller size as well as to attempt different flow methods and investigate stationary phase asymmetry to create a truly two-dimensional platform.

Chapter 5

Surface Modification of Silicon Pillar Arrays to Enhance Fluorescence Detection of Uranium and DNA

5.1 – Abstract

There is an ever-growing need for detection methods that are both sensitive and efficient, such that reagent and sample consumption is minimized. Nanopillar arrays fit this need due to their scale and their field enhancement effects. This work investigates the use of nanopillar arrays for the detection of uranyl ion and of DNA, two analytes unalike but for their low quantum efficiencies and the need for high-throughput analyses. The adaptability of these platforms was apparent, as methods for the surface immobilization of both analytes were developed. The limit of detection for uranyl ion on this system was determined to be less than 1 ppm. Moreover, differentiation between single-strand and double-strand DNA was possible, including qualitative identification between double-stranded DNA and DNA of the same sequence, but with a 10-base-pair mismatch.

5.2 – Introduction

Nanostructures have been the subject of a great deal of recent work due to the complex and unique nature of their optical properties.[75–78] Our own group has done research into the ability of nanopillars to act as field enhancers for fluorescence.[39,40,79] While nanopillars may be too large for quantum confinement effects, silicon pillars at or near 100 nm in diameter do exhibit optical resonances within the visible spectrum, making them valuable for fluorescence research.[33,75,76,80] Not only does the nanoscale platform of pillar arrays minimize reagent consumption and sample volumes, but the vertical geometry of the pillars and the capability of coating them with a porous surface increases the number of sites available to bind fluorophores within the same field of view. Additionally, it is possible to functionalize the surface with a wide variety of substrates via silane and other chemistries to facilitate the binding of analytes.

Events such as the nuclear disaster at the Fukushima Nuclear Power Plant in 2011 have and will continue to pose significant hurdles to traditional uranium detection and analysis, mostly due to the sheer number and variety of samples that need to be evaluated. Current approaches typically consist of solid phase extraction (SPE) followed by radiometric counting or ionization and mass analysis.[81–86] While these methods are ideal for trace level samples, method complexity as well as instrumentation investment, field portability, and footprint can be limiting and have driven the investigation into alternate methodologies. Herein, we examine using the coordinating compound N, N-diisobutyl-2-(octyl(phenyl)-phosphoryl) acetamide (CMPO), used in many actinide recovery resins, to capture uranyl (UO_2^{2+}) at the porous layer surface of silicon nanopillars for fluorescence detection. The waveguide enhancement of the nanopillars will work to combat the notoriously low quantum yield associated with uranyl, and the nature of the arrays mean that very small sample sizes may be used and analyzed quickly.

Similar advantages must be taken into consideration when entering the realm of bioanalytics. Like uranyl, nucleic acids exhibit low quantum yields, and very small sample sizes are frequently desired.[87] DNA quantitation has been accomplished in the literature by a variety of methods including UV absorbance spectroscopy and spectrofluorimetry.[88–91] There has also been recent progress using microfluidic chips in nucleic acid research as all-in-one platforms for processes such as ligation and digestion.[92–94] Denaturation and reassociation are important physiochemical processes of DNA, the study of which can provide valuable insight into not only the growth of cells and viruses but also the taxonomic and evolutionary relationships between organisms.[95] Reassociation of DNA was first measured by binding small fragments of labeled DNA to long strands immobilized in an agar-based supporting medium, a method later replaced with the use of a hypoxypatite column, on which double-stranded DNA is retained but single-

stranded DNA is not.[95,96] However, both of these methods are time- and labor-intensive, and while work has been done in an effort to reduce these time constraints, such as using size-selective capillary electrophoresis to separate double-stranded DNA samples,[96] to our knowledge a high-throughput method such as presented here has not been developed for the purpose of reassociation evaluation. Herein, we investigate the use of nanoscale pillar arrays for the detection of double- and single-stranded DNA via sequestration of the strands on the pillar surface and fluorescence measurement of added intercalating dyes.

5.3 – Experimental

Fabrication of EBL Arrays and Deposition of PSO

Electron beam lithography (EBL) pillar arrays were created using a previously reported process.[15,33,45] This process involved writing of the circular patterns in a positive tone electron beam resist (300 nm of Zep 520A), followed by vacuum deposition of a 20 nm chromium layer (VE-240, Thermonics Laboratory, Inc.) and metal lift-off in acetone to form a mask, and finally anisotropic reactive ion etching (RIE) of the silicon substrate not masked by chromium. The pattern of arrays on the wafer is shown in Figure 5.3.1. The arrays used for this study were 10 X 10 pillars with diameters ranging from 60-160 nm varying along a horizontal axis, and etched to create pillars the height of 1 ± 0.2 μm. Each array was separated from those adjacent by distances greater than 20 μm to avoid any possibility of optical coupling or crosstalk.

The structure of the pillars was confirmed with scanning electron microscope (SEM) images obtained with a Merlin (Carl Zeiss) microscope with a field-emission gun operating at approximately 3 kV. Wafers were then annealed in 10% H_2 in Ar under atmospheric pressure at 800°C for 15 min in a cold wall furnace (FirstNano) to remove any residual organics from the pillar arrays.

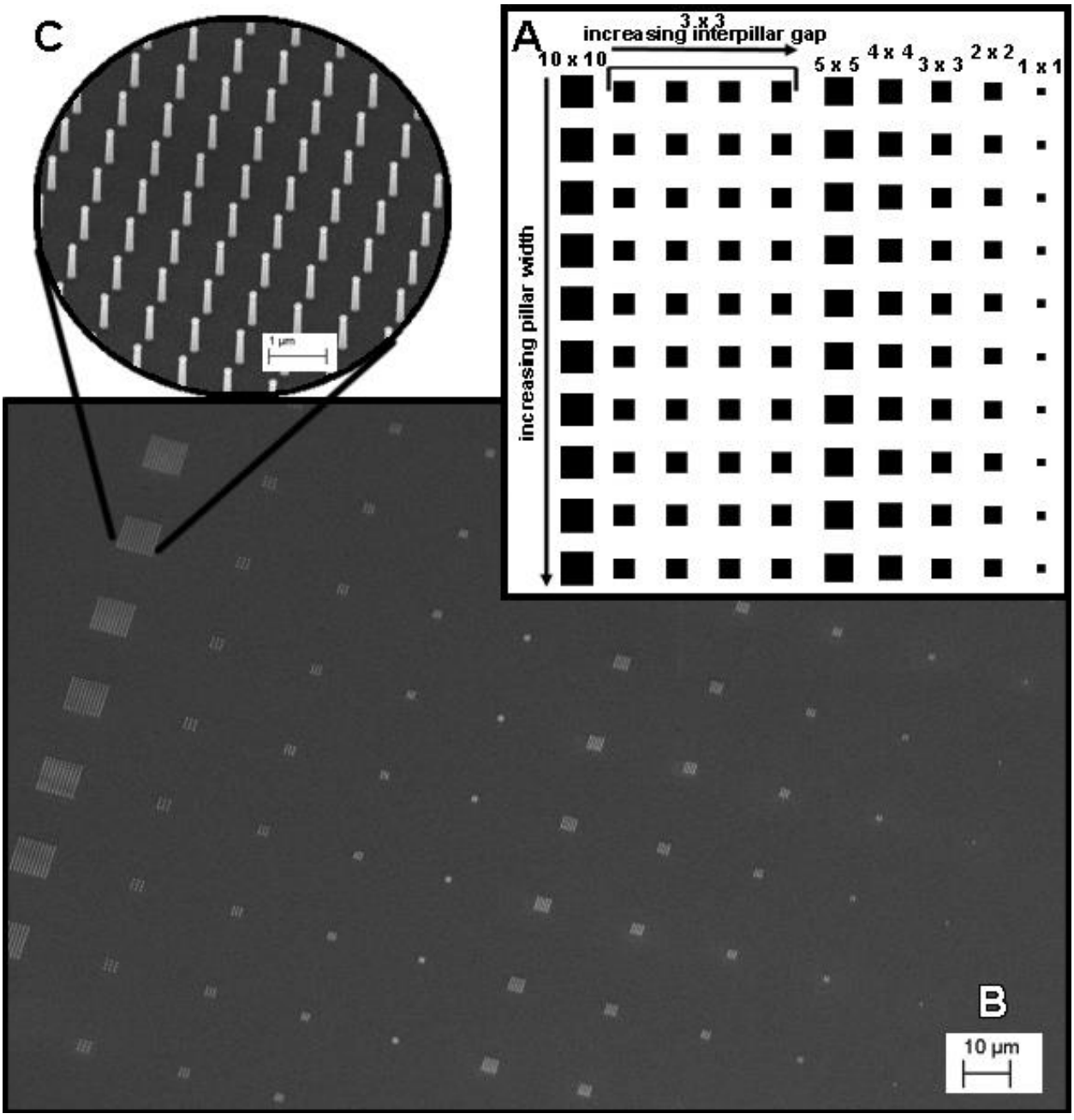

Figure 5.3.1: Layout of the EBL arrays used is shown in (**A**), with an SEM image of the created arrays in (**B**). Inset (**C**) shows a close-up of one of the 10 pillar x 10 pillar arrays within this larger array of arrays.

The PSO coating was accomplished via room temperature plasma enhanced chemical vapor deposition (PECVD, Oxford Instruments) with the chamber temperature at 27 °C and pressure at 600 mTorr.[41,59,97] Deposited thicknesses included 5 nm, 10 nm, or 25 nm of PSO.

Determination of Ideal Pillar Widths

While using the precise control of pillar geometries afforded by the EBL fabrication would create a system whereby the enhancement of the analyte could be evaluated and optimized, the EBL approach requires expensive equipment and is a slow serial process, creating practical limits as to the size and quantity of fabricated arrays. Therefore, pillar arrays created via the EBL fabrication method are unfeasible as platforms due to the time and monetary demands of a high throughput analytical method. In order to meet these high demands, we decided to use a platform that may compromise some of the optimized enhancement for quickly fabricated vast pillar array substrates—namely, stochastic platinum dewetted (DW) pillar arrays, whose usefulness has been previously expounded upon.[15,40,45] To create these arrays, we first needed to determine the optimum pillar diameter range.

To this end, EBL arrays with a range of pillar diameters were first functionalized with 3-aminopropyltriethoxysilane (APTES) by placing the pieces in a 10% v/v APTES/toluene solution and soaking at room temperature for 1 hr. The pieces were then sequentially rinsed with toluene, methanol, and deionized water and then were soaked in 1 mM fluoresceinisothiocyanate (FITC) (in ethanol) for 45 min. After a triplicate rinse in ethanol to remove any excess FITC, fluorescence imaging of the pieces was performed with a Nikon Eclipse E600 microscope and Q-capture software.

Fabrication of Dewet Pillars and Deposition of PSO

To create high-throughput U platforms, we created silicon nanopillar arrays using the thermal DW of a Pt film process previously developed.[40,45,98] This method begins with physical

vapor deposition of a thin, 8 nm Pt film (Thermonics Laboratory, VE-240) on a p-type silicon wafer with 100 nm of thermally grown SiO_2. During the Pt deposition, the deposition rate and the average (mass-based) thickness of the deposited metal were monitored with a quartz-crystal microbalance. The platinum film was then thermally annealed in a 10:1 mixture of argon and hydrogen at 735 Torr in a cold wall furnace (Easy Tube 3000, First Nano, Ronkonkoma, NY) equipped with a radiative heat source. During the anneal step the heat source was set to its maximum power (22 kW) for 8 s yielding an estimated maximum substrate temperature of 900 °C.

The thermally induced metal-film dewetting created nonuniform circular masking patterns. These platinum islands were subsequently used as a selective mask for RIE (Oxford PlasmaLab, Oxford Instruments, UK). In each process the RIE was tuned via power, pressure, temperature, time, and plasma composition (argon, sulfur hexafluoride, and octafluorocyclobutane) to achieve the desired etching profile of close to vertical and depth of approximately 1 μm. Finally, pillars were coated with 5 nm PSO by PECVD and then imaged via SEM.

Functionalization of the Surface for Uranyl Detection

The final surface functionalization for the extraction of the uranyl ion onto the nanopillar surface follows a procedure previously established in a patent, until the final TEOS deposition.[99] This method coats the silicon surface with CMPO, a common actinide binding agent, by combining it with 3-aminopropyltriethoxysilane (APTES). First, arrays were acid bathed in 50:50 sulfuric:nitric acid for 30 minutes and dried overnight at 80 °C. Then, 0.05 g of CMPO was dissolved in 25 mL of ethanol, at which point pillar arrays were added and the solution was stirred for 90 min. Care was taken to ensure that the stirring did not cause any direct impact with the pillar array surface. Subsequently, 5 mL of 1 mM APTES was added to the solution and

stirred for an additional 120 min under ambient nitrogen. Then the substrate was removed from the solution and dried under nitrogen.

A layer of tetraethyl orthosilicate (TEOS) was then added. When the patent[99] was followed from this point, and the addition of TEOS was done in solution, some heavy polymerization of the siloxane compounds was observed via SEM analysis. This polymerization both caused damage to the pillar arrays and created a nonuniform pillar array surface. In order to combat this polymerization, the TEOS layer was deposited via a vapor phase by placing the array under vacuum overnight with a reservoir of TEOS. The substrate was then rinsed in triplicate by each toluene, tetrahydrofuran (THF), ethanol, and deionized water. In order to create a hydrophobic surface for spotting purposes, the array was placed under vacuum overnight with a reservoir of 1:10 N-butyldimethylchlorosilane (C4):toluene, after which the array was rinsed for a final time in duplicate with toluene, THF, 10:90 THF:water, and deionized water.

In order to determine if the CMPO was acting as intended by sequestering and dispersing the uranyl throughout the delivered spots, arrays were also functionalized with only C4 for comparison. To do this, arrays were acid bathed and dried as above, and then placed under vacuum overnight with a reservoir of 1:10 C4:toluene before being rinsed.

Detection of Uranyl

A 1000 μg/mL (1000 ppm) stock solution of uranyl nitrate hexahydrate (SPI Supplies) in 5% HNO_3 (High Purity Standards, Lot 604605) was created and diluted to form sample solutions containing 1, 25, 50, 75, 100, 200, 300, 400, and 500 μg/mL uranyl in 5% HNO_3. These were then spotted onto the dewet arrays functionalized with CMPO and dewet arrays functionalized with only C4, in volumes of 0.2 μL and in triplicate.

The fluorescence images were taken with a Nikon Eclipse LV150 microscope using the 10X objective. The microscope was equipped with a halogen-amp light source, a multicolor

fluorescence cube (DAPI-FITC-TRITC), and a color CCD camera (DS-2M, Nikon, Inc.) controlled by NIS-Elements software. Fluorescence color (RGB) images with 16-bit color depth per channel were acquired by integrating a sequence of 16 8-bit color images. The blue-light excitation was used with the same collection time (20 s), gain (2), and offset (-500) for both background and sample measurements.

Images were analyzed using ImageJ software. The signal was integrated over a circular area with a diameter equal to the largest spot. This was done by centering the area on each spot and integrating the intensity via ImageJ software. All data were background corrected by subtracting the intensity produced by the surface without uranyl surrounding the spots. The standard deviations and averages of the intensities for each concentration were then calculated and plotted against concentration to obtain a linear relationship.

Upon first evaluation, there was a lack of luminescence and we surmised that the native fluorescence of the $(UO_2)^{2+}$ was either too weak or being quenched by the system. However, recent work has been done in aqueous samples with a reagent called Uraplex™, a uranium complexant which extends the lifetime and minimizes quenching of $(UO_2)^{2+}$.[100] As such, it was decided to use this complexant with our samples. Uraplex™ concentrate (Chemchek Instruments) was diluted 1:20 in deionized water and then incorporated as 50% of the sample mixtures by volume.

Functionalization of the Surface for DNA detection

Our procedure for functionalization of the pillar surface for the immobilization of DNA is based upon work previously done by Yang et al.[92] A schematic of the process is shown in Figure 5.3.2. First the arrays were acid bathed and dried as above. Then, arrays were functionalized with APTES and rinsed as above. Arrays were then soaked in a 10 μg/mL solution of sulfo-N-hydroxysuccinimide (NHS)-biotin in phosphate-buffered saline (PBS, 1X, pH 7.4) for 1 hr at

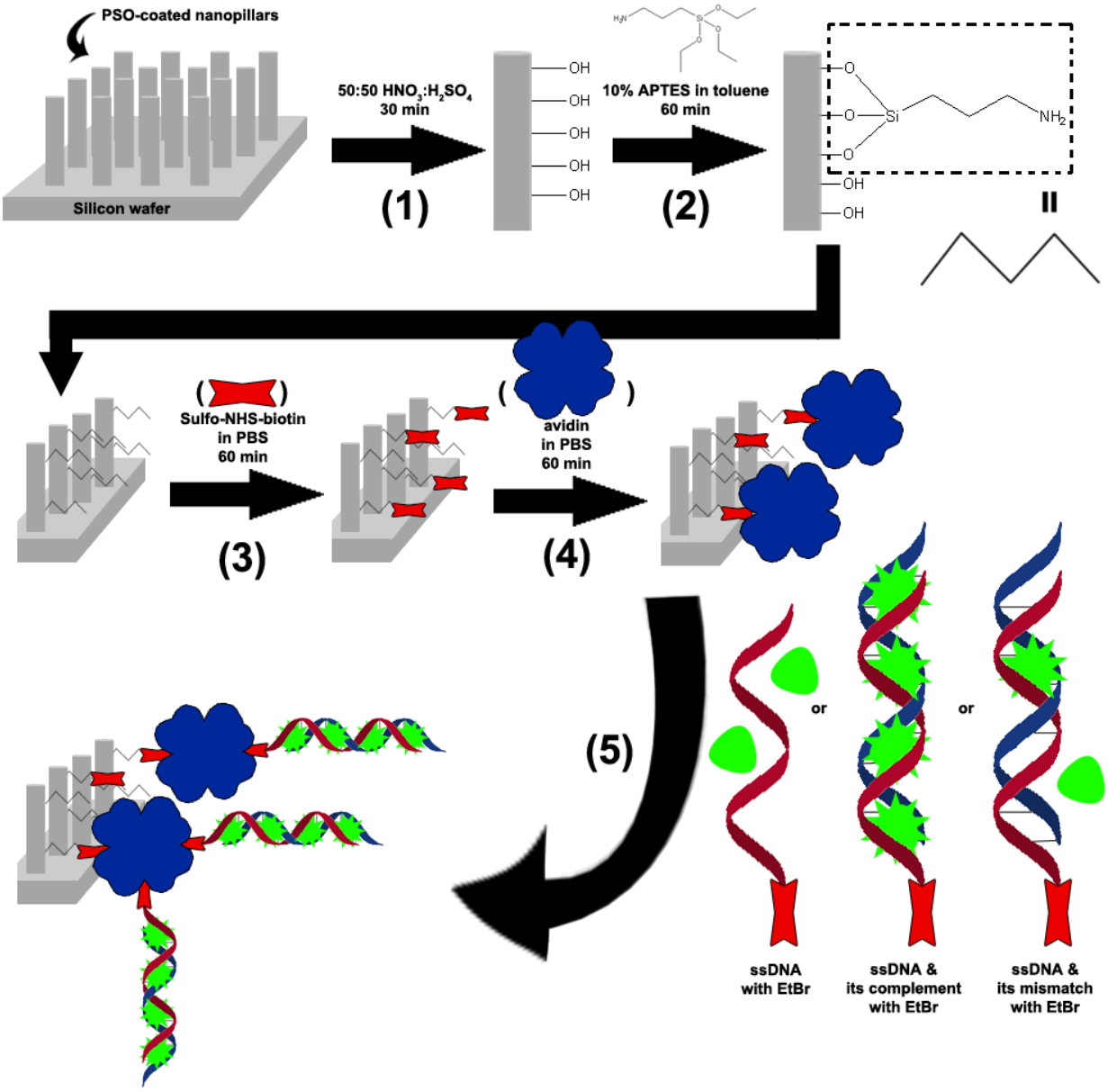

Figure 5.3.2: Functinalization sequence for immobilization of DNA on the pillar surface. Pillars are acid bathed (**1**), then functionalized with APTES (**2**). They are biotinylated by addition of sulfo-NHS-biotin (**3**) and addition of avidin (**4**) completes the extraction surface. When DNA solutions are introduced (**5**), the biotinylated DNA strands are bound by the avidin-functionalized pillars.

room temperature. After rinsing in triplicate with additional 1X PBS, arrays were dried under nitrogen and then soaked in 1 μg/mL streptavidin in PBS (1X, pH 7.4) for 1 hr at room temperature. Finally, arrays were rinsed in triplicate with 1X PBS and then dried under nitrogen. To discourage denaturing, arrays were stored at 4 °C until used.

Detection of DNA

Three single-strand DNA (ssDNA) 100-base-pair oligomers were designed and obtained from Invitrogen. The first was biotin-terminated so that it could be bound to the pillar array surface via the strong biotin-avidin affinity ($K_{affinity} \sim 10^{15}$). The other two oligomers were the exact complement of the first and the complement with a 10-base pair mismatch scattered throughout the strand, respectively. The oligomers were reconstituted in 1 mL of Tris-EDTA buffer (TE, 1X, pH 8). Four different solutions were then created to produce samples with a 5:1 base pair:dye molecule ratio and ~60 nM DNA concentrations in TE buffer. These solutions consisted of the biotinylated ssDNA ("alone"), the biotinylated ssDNA with its complement ("matched"), the biotinylated ssDNA with the complement containing 10-base pair mismatches ("mismatched"), and a dye blank. The intercalating dye used was ethidium bromide (EtBr, Sigma Aldrich, 1.15×10^{-5} M). These solutions were allowed to incubate for 1 hr at room temperature before being used or being stored at 4 °C for later use.

DNA solutions were then applied to avidin-functionalized arrays in one of two ways, either by spotting or soaking. For application by spotting, 0.1 μL of sample was applied to the array surface and allowed to dry. The spots were then imaged, rinsed with ~1 mL 1X PBS buffer, and imaged again. For application by soaking, ~100 μL of sample was applied to the surface of the array, with surface tension keeping it in droplet form over the entire array surface, and allowed to soak for 1 hr at room temperature. The array was then imaged, rinsed with ~1 mL 1X PBS buffer, and imaged again. The same Nikon microscope as was used for the uranyl

detection was used here, but with the green-light excitation for EtBr detection. The same collection time (5 s), gain (2), and offset (-500) were used for both background and sample measurements.

Images were analyzed using ImageJ software. The signal was integrated over a circular area with a diameter equal to the largest sample spot. This is done by centering the area on each spot and integrating the intensity via ImageJ software. In spotted arrays, the signal was background-corrected by subtracting the integrated signal within the same-sized circular area where there was no sample applied.

5.4 – Results and Discussion

Determination of optimal pillar width and comparison to flat silicon

Figure 5.4.1 shows arrays with pillar diameters ranging from 60-100 nm and with either 5, 10, or 25 nm of PSO, after being soaked in FITC, rinsed, and imaged. It was determined that 80-90 nm diameter pillars with 5 nm of PSO showed the greatest fluorescence with the least amount of background, and so fabrication parameters that would create approximately this size were used for the fabrication of the dewet pillars for uranyl and DNA analysis. In using this EBL wafer layout, we also were able to demonstrate the large on-to-off-pillar ratio of the fluorescence signal. This ratio decreases as pillar width deviates from the optimum and as PSO thickness increases. With pillar thicknesses greater than 100 nm and PSO thicknesses of 25 nm or greater, the effect is nullified and the fluorescence signal on flat silicon can even become greater than that on pillars. The thickness of the PSO determines the measured on/off pillar ratio. For instance, we measured an off-pillar signal of zero for 5 nm PSO on 60-100 nm pillar diameters, but for 10 nm PSO on 80 nm pillars, we were able to calculate an on/off pillar ratio of 3.92.

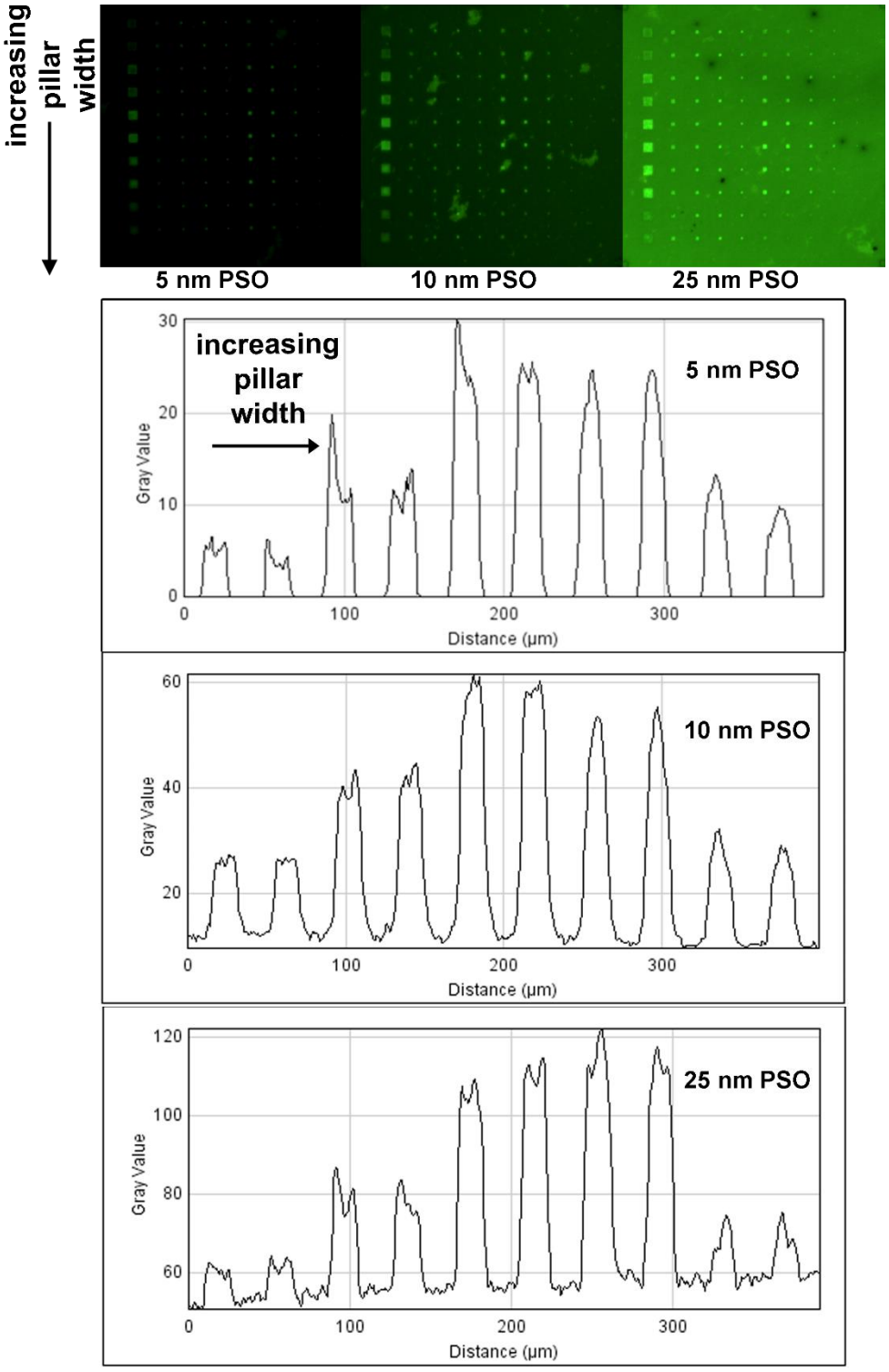

Figure 5.4.1: Fluorescence microscope images of EBL pillars functionalized with APTES and soaked with FITC to determine optimum pillar width and PSO thickness are shown at the top, with pillar width increasing down the array, every other pillar in increments of 10 nm, from 60 nm to 100 nm. Below that are the plot profiles depicting fluorescence intensity for the 10 pillar x 10 pillar arrays pictured.

Detection of uranyl

The comparison of CMPO and C4 on the pillar surface for uranyl detection can be seen in Figure 5.4.2. Surprisingly, we did not observe a difference between uranyl spotted on CMPO and uranyl spotted on C4. While we designed the CMPO functionalization to sequester the uranyl, and so expected it to produce smoother, more even spots, we observed the same effect with C4. After rinsing the arrays and re-imaging them, we found that the C4 array seemed to retain more of the uranyl than the CMPO did. This is possibly due to the decreased wettability of the C4 array, as it exhibited more hydrophobic coverage. This was one of the biggest tradeoffs between the CMPO versus the C4 method, because while we finished the CMPO functionalization with a C4 layer, it is likely that it did not produce as much coverage as in the traditional method where it has access to all the free hydroxyls. It is possible that soaking the arrays in the uranyl solutions may allow for more interaction between the stationary phase and the analyte, producing a different result.

Figure 5.4.3 shows the range of uranyl concentrations when spotted on CMPO arrays and their respective intensity profiles, and the corresponding calibration curve, which plots the background-corrected average integrated density of each spot versus its concentration. Regression analysis indicated that the experimental data closely fit the linear statistical model between 0 and 200 ppm, with a coefficient of determination (R^2) of 0.9842. Over 200 ppm, oversaturation of the signal resulted in not only a leveling out of the calibration curve, but also a significant increase in error, from an average of 1×10^9 to an average of 4×10^9. The noise of the blank was used to determine figures of merit. The limit of detection was calculated as 0.969 ppm, which while ~3 orders of magnitude less sensitive than other research using Uraplex™, is still practical for screening high concentrations of uranyl.[100] Furthermore, the more sensitive techniques using this complexant also used time-resolved pulsed laser detection, not simple

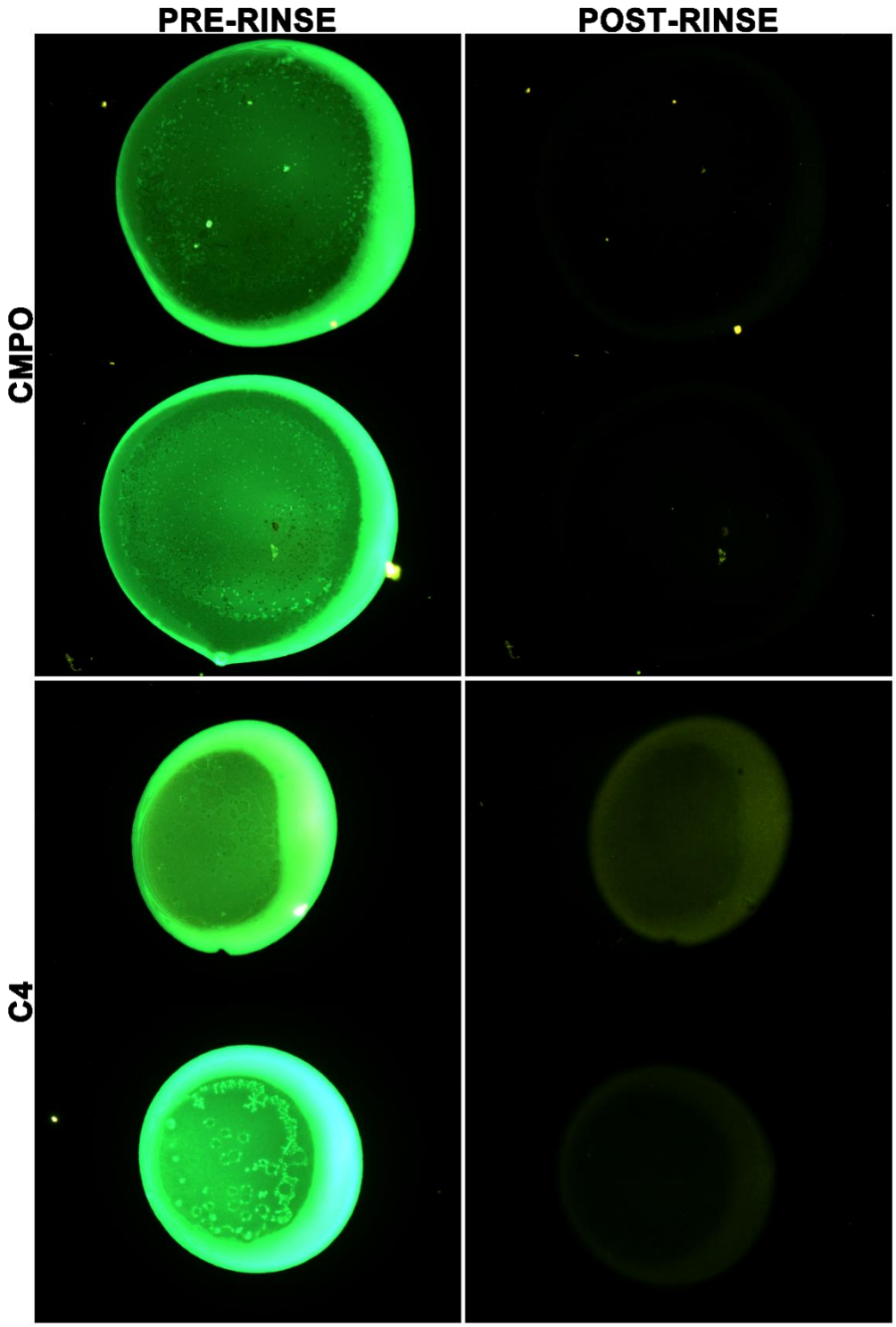

Figure 5.4.2: Depiction of 100 and 200 ppm uranyl spotted on CMPO (top) and C4 (bottom) arrays, pre-rinse (left) and post-rinse (right).

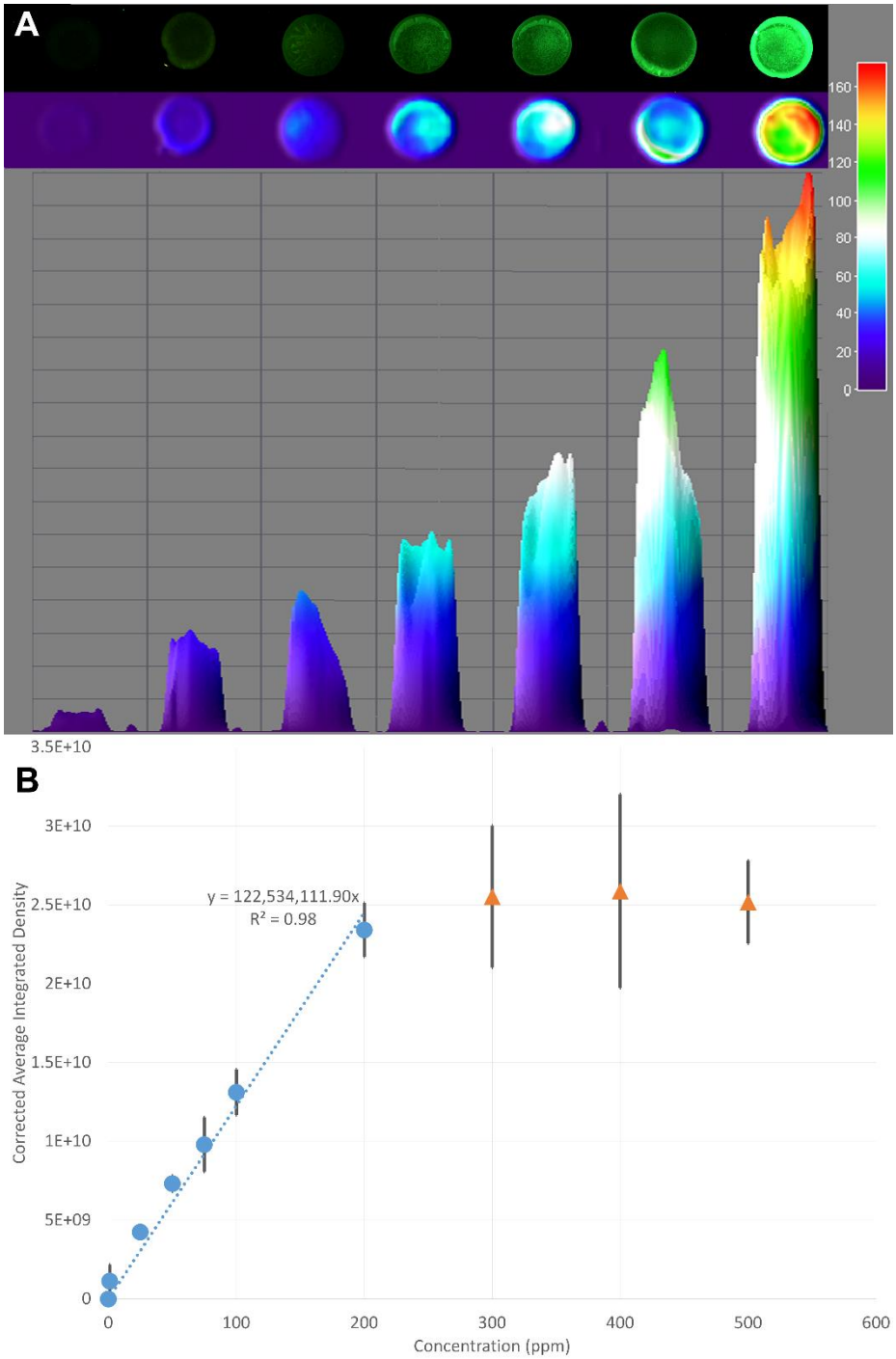

Figure 5.4.3: Fluorescence microscope images of uranyl spotted on dewet arrays functionalized with CMPO are shown in (**A**) with corresponding heat maps below, where redder color indicates greater fluorescence signal intensity. Concentration increases from left to right: blank, 1 ppm, 25 ppm, 50 ppm, 75 ppm, 100 ppm, and 200 ppm. (**B**) shows the calibration curve for these samples. The blue circles represent the images shown here, where the curve exhibits linearity. The orange triangles represent the signals measured for 300 ppm, 400 ppm, and 500 ppm, where oversaturation of signal caused the intensity to level out.

fluorescence, and we believe that if that method of detection were combined with our system, similar or lower limits could be achieved.

Detection of DNA

It was quickly determined that spotting was unfeasible as an application method. The arrays did not exhibit enough of a hydrophobic nature to allow for the sample to concentrate within a small area. When the droplet made contact with the array surface, it immediately wicked through the pillars and spread to an area ≥2 mm in diameter, greater than the field of view on the fluorescence microscope, and dried with significant coffee-ring effect. Additionally, while fluorescence was visible immediately after spotting, it was not resistant to rinsing, resulting in negligible signal post-rinse.

Application by soaking, however, resulted in even coverage across the array and quantifiable fluorescence even after rinsing. Indeed, rinsing appeared to be necessary, as pre-rinse, the different solutions all exhibited the same fluorescence, indicating that there were large amounts of excess dye. The difference between pre- and post-rinse, as well as the differences between the different solutions, are illustrated in Figure 5.4.4. The average integrated densities of the arrays pre- and post-rinse are also shown in the figure. For EtBr, the matched solution of the ssDNA and its exact complement exhibited approximately 175% the fluorescence of the alone solution, while the mismatched solution of the ssDNA and its 10-BP-mismatched complement exhibited 105% the fluorescence of the alone solution (and 60% the magnitude of the matched signal). It is possible that the fluorescence of the alone solution is artificially high due to self-hybridization of the single strand or possible electrostatic interaction of EtBr with ssDNA,[101] as the signal of the alone solution was roughly four times that of the blank. If no hybridization were present, we would expect the two signals to be more similar. We also hypothesize that the fluorescence of the mismatched solution is affected by the way that the EtBr

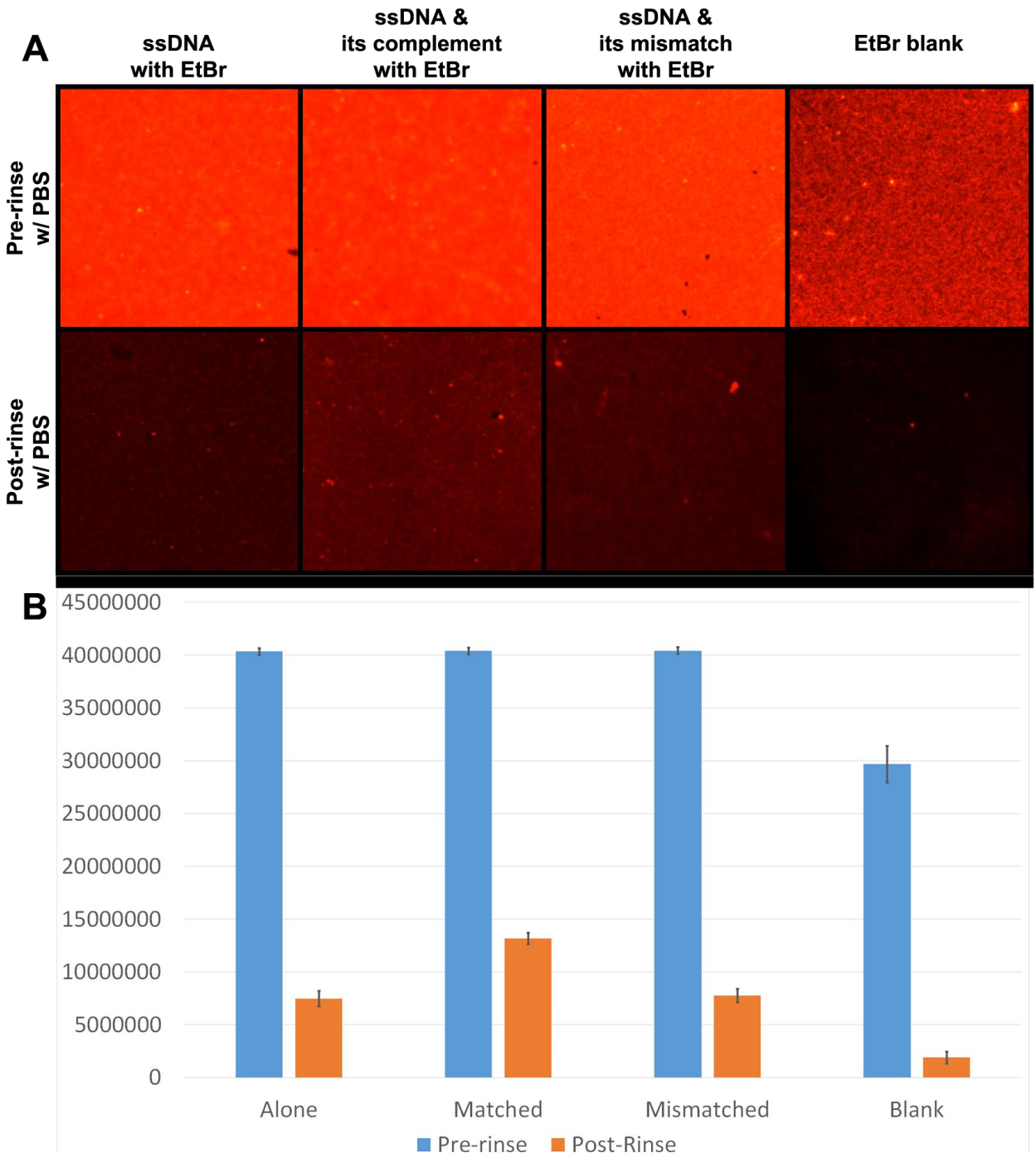

Figure 5.4.4: Fluorescent images of sample areas on pillar arrays functionalized for DNA immobilization and soaked with one of the four DNA solutions are shown in (**A**). Sample areas are shown pre- (top) and post- (bottom) rinse. (**B**) graphs the fluorescence intensity measured for each of these eight samples.

is able to intercalate with the mismatched strands. The mismatches between the strands were designed such that no portion of the strands were mismatched by more than three base pairs, so we don't expect that the signal is articicially high due to self-hybridization. However, it could be that the mismatches are insufficient to prevent EtBr from binding, resulting in a signal which is greater than anticipated.

5.5 – Conclusions About Surface Modification for Uranium and DNA Detection

In this work, we have introduced two surface chemistry approaches for the detection of uranyl ion and of DNA that are ideal to use as high-throughput screening methods. Both methods consisted of creating a multilayer extraction resin on silicon nanopillar systems. In the case of uranyl, this allowed for the fast analysis of many samples at sub-ppm concentrations using sub-μL volumes, which while not as sensitive as other methods using Uraplex^{TM}, could still be used for screening purposes. In the case of DNA, this allowed for the differentiation between picomole amounts of single-stranded and double-stranded DNA, including identification of base-pair mismatches. The retention of sensitivity while using minimal sample and reagent volumes, and the lack of complex and highly specific instrumentation combine to create a platform that is both accessible and economically advantageous.

Chapter 6

Conclusion

6.1 – Concluding Remarks

Micro- and nano-structured on-chip media created via silicon wafer microfabrication technology have a wide range of possible applications. [21] Notably, they have been used to create microstructures that can not only function as an alternative to the traditional stationary phases used in liquid chromatography columns, but also can be used to create capillary-action driven, open or pressure-driven, enclosed planar chromatography systems.[23–31] Not only do these systems exhibit much greater uniformity, due to the ability to exactly control of the layout and nature of the features, but they also do not exhibit the great decrease in mobile phase velocity with increasing solvent front distance like in TLC. As such, they can exhibit much greater efficiency than other planar chromatography systems.[21]

The greatest limitation of these pillar arrays as separation systems is their limited surface area. Therefore, we investigated two different surface coatings to create a more porous phase. The first, petal-like carbon, showed promise due to its seemingly fibrous nature and unique chemistries, but ultimately quenched fluorescence too much to be useful for these systems. The second, porous silicon oxide (PSO), demonstrably increased the surface area of our arrays and increased retention. Using PSO, we created a system not only viable for one-dimensional separations, but also those in two dimensions.

It was previously established by others that when taken into the nanoscale regime, these pillar array systems can not only be used for separations, but also exhibit fluorescence-enhancement properties that can greatly increase their applicability. While nanopillars may be too large for quantum confinement effects, silicon pillars at or near 100 nm in diameter do exhibit optical resonances within the visible spectrum, making them valuable for fluorescence research.[33,75,76,80] Previous research modified the pillar surface to enhance the fluorescence of

beryllium.[40] In the work discussed in this dissertation, we followed the logical extension of those results and created two multi-layer immobilizing phases for the detection of uranyl ion and of DNA. Quantitation of both of these analytes typically requires time- and labor-consuming processes, and so we aimed to create high-throughput methods to allow for rapid detection. Using a method to create stochastic, platinum-dewetted pillar arrays instead of deterministic, electron-beam lithography pillar arrays, we dramatically decreased the monetary and labor costs of fabrication. Once functionalized, these arrays allowed us to detect uranyl samples at sub-ppm concentrations using sub-μL volumes and differentiate between picomole amounts of single-stranded and double-stranded DNA, including identification of base-pair mismatches.

Although the two uses of pillar arrays presented here appear different, that only serves to highlight the diversity of the applications possible with these systems. By changing the size and the surface of the pillars, we created entirely new systems optimized for a variety of uses. What these systems do have in common is that they are fast, efficient methods for the detection and identification of samples.

References

(1) Kirchner, J. G.; Miller, J. M.; Keller, G. J. *Anal. Chem.* **1951**, *23* (3), 420–425.

(2) Miller, J. M.; Kirchner, J. G. *Anal. Chem.* **1954**, *26*, 2002.

(3) Miller, J. M.; Kirchner, J. G. *Anal. Chem.* **1952**, *24* (9), 1480–1482.

(4) Stahl, E. *Chemiker-Zeitung* **1958**, *82*, 323.

(5) Touchstone, J. C. *Practice of Thin-Layer Chromatography*, 3rd ed.; John Wiley & Sons, INC: New York, 1992.

(6) Miller, J. M. *Chromatography: Concepts and Contrasts*, 2nd ed.; John Wiley & Sons, INC: Hoboken, NJ, 2005.

(7) Poole, S. K.; Poole, C. F. *J. Chromatogr. A* **2011**, *1218* (19), 2648–2660.

(8) Frolova, A. M.; Chukhlieb, M. A.; Drobot, A. V; Kryshtal, A. P.; Loginova, L. P.; Boichenko, A. P. *Open Surf. Sci. J.* **2009**, *1*, 40–45.

(9) Bezuidenhout, L. W.; Brett, M. J. *J. Chromatogr. A* **2008**, *1183* (1–2), 179–185.

(10) Jim, S. R.; Taschuk, M. T.; Morlock, G. E.; Bezuidenhout, L. W.; Schwack, W.; Brett, M. J. *Anal. Chem.* **2010**, *82* (12), 5349–5356.

(11) Morlock, G. E.; Oellig, C.; Bezuidenhout, L. W.; Brett, M. J.; Schwack, W. *Anal. Chem.* **2010**, *82* (7), 2940–2946.

(12) Clark, J. E.; Olesik, S. V. *Anal. Chem.* **2009**, *81* (10), 4121–4129.

(13) Gocan, S. In *Encyclopedia of Chromatography, Volume 1*; Cazes, J., Ed.; Taylor anf Francis Group, LLC: Boca Raton, FL, 2010; pp 730–735.

(14) Snyder, L. R. *J. Chromatogr.* **1974**, *92*, 223–230.

(15) Kirchner, T. B.; Strickhouser, R. B.; Hatab, N. a.; Charlton, J. J.; Kravchenko, I. I.; Lavrik, N. V.; Sepaniak, M. J. *Analyst* **2015**, *140* (10), 3347–3351.

(16) Fairbairn, J. W.; Relph, S. J. *J. Chromatogr.* **1968**, *33*, 494–499.

(17) Fenimore, D. C.; Meyer, C. J. *J. Chromatogr.* **1979**, *186*, 555–561.

(18) Koishi, T.; Yasuoka, K.; Fujikawa, S.; Ebisuzaki, T.; Zeng, X. C. *Proc. Natl. Acad. Sci. U. S. A.* **2009**, *106* (21), 8435–8440.

(19) Walworth, M. J. Liquid Extraction Based Surface Sampling: Liquid Microjunction Surface Sampling Probes Coupled with Mass Spectrometry, University of Tennessee, 2011.

(20) Crane, N. A.; Lavrik, N. V.; Sepaniak, M. J. *Analyst* **2016**, *141* (4), 1239–1245.

(21) Kirchner, T. B.; Hatab, N. A.; Lavrik, N. V.; Sepaniak, M. J. *Anal. Chem.* **2013**, *85* (24), 11802–11808.

(22) Giddings, J. C. In *Unified Separation Science*; John Wiley & Sons, INC: New York, NY, 1991.

(23) He, B.; Tait, N.; Regnier, F. *Anal. Chem.* **1998**, *70* (18), 3790–3797.

(24) Gzil, P.; Vervoort, N.; Baron, G. V.; Desmet, G. *Anal. Chem.* **2003**, *75* (22), 6244–6250.

(25) De Malsche, W.; Eghbali, H.; Clicq, D.; Vangelooven, J.; Gardeniers, H.; Desmet, G. *Anal. Chem.* **2007**, *79* (15), 5915–5926.

(26) Patel, R. B.; Gopani, M. C.; Patel, M. R. *Chromatographia* **2013**, *76* (19–20), 1225–1231.

(27) Malsche, W. De; Bruyne, S. De; Beeck, J. Op De; Eeltink, S.; Detobel, F.; Gardeniers, H.; Desmet, G. *J. Sep. Sci.* **2012**, *35* (16), 2010–2017.

(28) Eghbali, H.; De Malsche, W.; Clicq, D.; Gardeniers, H.; Desmet, G. *LC-GC Eur.* **2007**, *20* (April 2007), 208–222.

(29) Lavrik, N. V; Taylor, L. C.; Sepaniak, M. J. *Lab Chip* **2010**, *10* (8), 1086–1094.

(30) Lavrik, N. V.; Taylor, L. T.; Sepaniak, M. J. *Anal. Chim. Acta* **2011**, *694* (1–2), 6–20.

(31) De Malsche, W.; De Bruyne, S.; Op De Beek, J.; Sandra, P.; Gardeniers, H.; Desmet, G.; Lynen, F. *J. Chromatogr. A* **2012**, *1230*, 41–47.

(32) Taylor, L. C.; Lavrik, N. V.; Sepaniak, M. J. *Anal. Chem.* **2010**, *82* (22), 9549–9556.

(33) Kandziolka, M.; Charlton, J. J.; Kravchenko, I. I.; Bradshaw, J. a.; Merkulov, I. a.; Sepaniak, M. J.; Lavrik, N. V. *Anal. Chem.* **2013**, *85* (19), 9031–9038.

(34) Poole, C. F. *J. Chromatogr. A* **2003**, *1000* (1–2), 963–984.

(35) Sherma, J. *Anal. Chem.* **2004**, *76* (12), 3251–3262.

(36) Kirchner, T. B. "The fabrication of micro- and nano-scale deterministic and stochastic pillar arrays for planar separations," The University of Tennessee, 2015.

(37) *Nanofabrication Handbook*; Cabrini, S., Kawata, S., Eds.; CRC Press: Boca Raton, FL, 2012.

(38) Mack, C. *Fundamental Principles of Optical Lithography: The Science of Microfabrication*; Wiley: Hoboken, NJ, 2007.

(39) Wells, S. M.; Merkulov, I. A.; Kravchenko, I. I.; Lavrik, N. V.; Sepaniak, M. J. *ACS Nano* **2012**, *6* (4), 2948–2959.

(40) Charlton, J. J.; Jones, N. C.; Wallace, R. A.; Smithwick, R. W.; Bradshaw, J. A.; Kravchenko, I. I.; Lavrik, N. V.; Sepaniak, M. J. *Anal. Chem.* **2015**, *87* (13), 6814–6821.

(41) Charlton, J. J.; Lavrik, N.; Bradshaw, J. A.; Sepaniak, M. J. *ACS Appl. Mater. Interfaces* **2014**, *6* (20), 17894–17901.

(42) Jansen, H. V; de Boer, M. J.; Unnikrishnan, S.; Louwerse, M. C.; Elwenspoek, M. C. *J. Micromechanics Microengineering* **2009**, *19* (3), 33001.

(43) Giaquinto, a.; Liu, Z.; Bach, A.; Kazakevich, Y. *Anal. Chem.* **2008**, *80* (16), 6358–6364.

(44) Ceiler Jr., M. F.; Kohl, P. A.; Bidstrup, S. A. *J. Electrochem. Soc.* **1995**, *142* (6), 2067–

2071.

(45) Charlton, J. J.; Lavrik, N.; Bradshaw, J. A.; Sepaniak, M. J. *ACS Appl. Mater. Interfaces* **2014**, *6*, 17894–17901.

(46) Knox, J. H.; Unger, K. K.; Mueller, H. *J. Liq. Chromatogr. Relat. Technol.* **1983**, *6*, 1–36.

(47) Pereira, L. *J. Liq. Chromatogr. Relat. Technol.* **2008**, *31* (11), 1687–1731.

(48) West, C.; Elfakir, C.; Lafosse, M. *J. Chromatogr. A* **2010**, *1217* (19), 3201–3216.

(49) Monser, L.; Darghouth, F. *J. Pharm. Biomed. Anal.* **2000**, *23* (2–3), 353–362.

(50) Lim, C. K. *Biomed. Chromatogr.* **1989**, *3* (2), 92–93.

(51) Chaimbault, P.; Petritis, K.; Elfakir, C.; Dreux, M. *J. Chromatogr. A* **2000**, *870* (1–2), 245–254.

(52) Gu, G.; Lim, C. K. *J. Chromatogr. A* **1990**, *515* (C), 183–192.

(53) Guiochon, G.; Siouffi, A.; Engelhardt, H.; Halasz, I. *J. Chromatogr. Sci.* **1978**, *16* (4), 152–157.

(54) De Malsche, W.; Clicq, D.; Verdoold, V.; Gzil, P.; Desmet, G.; Gardeniers, H. *Lab Chip* **2007**, *7* (12), 1705–1711.

(55) De Smet, J.; Gzil, P.; Vervoort, M.; Verelst, H.; Baron, G. V.; Desmet, G. *Anal. Chem.* **2004**, *76* (13), 3716–3726.

(56) Schure, M. R.; Maier, R. S.; Kroll, D. M.; Davis, H. T. *J. Chromatogr. A* **2004**, *1031* (1–2), 79–86.

(57) Kirchert, S.; Wang, Z.; Taschuk, M. T.; Jim, S. R.; Brett, M. J.; Morlock, G. E. *Anal. Bioanal. Chem.* **2013**, *405* (23), 7195–7203.

(58) Kanyal, S. S.; Häbe, T. T.; Cushman, C. V.; Dhunna, M.; Roychowdhury, T.; Farnsworth, P. B.; Morlock, G. E.; Linford, M. R. *J. Chromatogr. A* **2015**, *1404*, 115–123.

(59) Detobel, F.; De Bruyne, S.; Vangelooven, J.; De Malsche, W.; Aerts, T.; Terryn, H.; Gardeniers, H.; Eeltink, S.; Desmet, G. *Anal. Chem.* **2010**, *82* (17), 7208–7217.

(60) De Malsche, W.; Gardeniers, H.; Desmet, G. *Anal. Chem.* **2008**, *80* (14), 5391–5400.

(61) Clicq, D.; Tjerkstra, R. W.; Gardeniers, J. G. E.; Van Den Berg, a.; Baron, G. V.; Desmet, G. *J. Chromatogr. A* **2004**, *1032* (1–2), 185–191.

(62) Tiggelaar, R. M.; Verdoold, V.; Eghbali, H.; Desmet, G.; Gardeniers, J. G. E. *Lab Chip* **2009**, *9* (3), 456–463.

(63) Freye, C. E.; Crane, N. a; Kirchner, T. B.; Sepaniak, M. J. *Anal. Chem.* **2013**, *85*, 3991–3998.

(64) Yang, P.; Liu, L.; Mo, J.; Yang, W. *Semicond. Sci. Technol.* **2010**, *25* (4), 45017.

(65) Snyder, L. R.; Kirkland, J. J. *Introduction to Modern Liquid Chromatography*, 2nd ed.;

John Wiley & Sons, INC: New York, 1979.

(66) Snyder, L. R.; Dolan, J. W.; Gant, J. R. *J. Chromatogr.* **1979**, *165*, 3–30.

(67) Dolan, J. W.; Gant, J. R.; Snyder, L. R. *J. Chromatogr.* **1979**, *165*, 31–58.

(68) DeVault, G. L.; Sepaniak, M. J. *J. Microcolumn Sep.* **2000**, *12* (7), 419–428.

(69) Safarik, D. J.; Eldridge, R. B. *Ind. Eng. Chem. Res.* **1998**, *37* (7), 2571–2581.

(70) Baker, B. B. *Inorg. Chem.* **1964**, *3* (2), 200–202.

(71) Yang, R. T.; Kikkinides, E. S. *AIChE J.* **1995**, *41* (3), 509–517.

(72) Williams, C. M.; Mander, L. N. *Tetrahedron* **2001**, *57* (3), 425–447.

(73) Mander, L. N.; Williams, C. M. *Tetrahedron* **2016**, *72* (9), 1133–1150.

(74) Giddings, J. C.; Keller, R. A. *J. Chromatogr.* **1959**, *2*, 626–633.

(75) Cao, L.; White, J. S.; Park, J.-S.; Schuller, J. A.; Clemens, B. M.; Brongersma, M. L. *Nat. Mater.* **2009**, *8* (8), 643–647.

(76) Cao, L.; Fan, P.; Barnard, E. S.; Brown, A. M.; Brongersma, M. L. *Nano Lett.* **2010**, *10* (7), 2649–2654.

(77) Seo, K.; Wober, M.; Steinvurzel, P.; Schonbrun, E.; Dan, Y.; Ellenbogen, T.; Crozier, K. B. *Nano Lett.* **2011**, *11* (4), 1851–1856.

(78) Walker, B. N.; Stolee, J. A.; Pickel, D. L.; Retterer, S. T.; Vertes, A. *J. Phys. Chem. C* **2010**, *114* (11), 4835–4840.

(79) Kandziolka, M.; Charlton, J. J.; Kravchenko, I. I.; Bradshaw, J. A.; Merkulov, I. A.; Sepaniak, M. J.; Lavrik, N. V. *Anal. Chem.* **2013**, *85* (19), 9031–9038.

(80) Wells, S. M.; Merkulov, I. a.; Kravchenko, I. I.; Lavrik, N. V.; Sepaniak, M. J. *ACS Nano* **2012**, *6* (4), 2948–2959.

(81) Chiarizia, R.; Horwitz, E. P.; Alexandratos, S. D.; Gula, M. J. *Diphonix® Resin: A Review of Its Properties and Applications*; 1997; Vol. 32.

(82) Chiarizia, R.; Horwitz, E. P.; Gatrone, R. C.; Alexandratos, S. D.; Trochimczuk, A. Q.; Crick, D. W. *Solvent Extr. Ion Exch.* **1993**, *11* (5), 967–985.

(83) Grate, J. W.; O'Hara, M. J.; Farawila, A. F.; Douglas, M.; Haney, M. M.; Petersen, S. L.; Maiti, T. C.; Aardahl, C. L. *Anal. Chem.* **2011**, *83* (23), 9086–9091.

(84) Horwitz, E. P.; Chiarizia, R.; Diamond, H.; Gatrone, R. C.; Alexandratos, S. D.; Trochimczuk, A. Q.; Crick, D. W. *Solvent Extr. Ion Exch.* **1993**, *11* (5), 943–966.

(85) Tagami, K.; Uchida, S. *Anal. Chim. Acta* **2007**, *592* (1), 101–105.

(86) Unsworth, E. R.; Cook, J. M.; Hill, S. J. *Anal. Chim. Acta* **2001**, *442* (1), 141–146.

(87) Clark, B. K.; Sepaniak, M. J. *J. Microcolumn Sep.* **1993**, *5* (3), 275–282.

(88) McGown, E. L. *Biotechniques* **2000**, *28* (1), 60–64.

(89) Ahn, S. J.; Costa, J.; Emanuel, J. R. *Nucleic Acids Res.* **1996**, *24* (13), 2623–2625.

(90) Haque, K. A.; Pfeiffer, R. M.; Beerman, M. B.; Struewing, J. P.; Chanock, S. J.; Bergen, A. W. *BMC Biotechnol.* **2003**, *3*, 20.

(91) Heid, C.; Stevens, J.; Livak, K. J.; Williams, P. M. *Genome Res.* **1996**, *6* (10), 986–994.

(92) Yang, F.; Zhang, Y.; Rafeah, S.; Ji, H.; Xie, S.; Ning, Y.; Zhang, G.-J. *RSC Adv.* **2014**, *4* (41), 21541.

(93) Wang, A.-B.; Cheng, C.-W.; Lin, I.-C.; Lu, F.-Y.; Tsai, H.-J.; Lin, C.-C.; Yang, C.-H.; Pan, P.-T.; Kuan, C.-C.; Chen, Y.-C.; Lin, Y.-W.; Chang, C.-N.; Wu, Y.-H.; Kurniawan, T.; Lin, C.-W.; Wo, A. M.; Chen, L.-C. *Electrophoresis* **2010**, *32* (3–4), 423–430.

(94) Xie, H.; Li, B.; Qin, J.; Huang, Z.; Zhu, Y.; Lin, B. *Electrophoresis* **2009**, *30* (20), 3514–3518.

(95) Britten, R. J.; Kohne, D. E. *Science (80-.).* **1968**, *161* (3841), 529–540.

(96) Li, Y.; White, J.; Stokes, D.; Sayler, G.; Sepaniak, M. *Biotechnol. Prog.* **2001**, *17* (2), 348–354.

(97) Lincoln, D. R.; Lavrik, N. V.; Kravchenko, I. I.; Sepaniak, M. J. *Anal. Chem.* **2016**, *88* (17), 8741–8748.

(98) Agapov, R. L.; Srijanto, B.; Fowler, C.; Briggs, D.; Lavrik, N. V; Sepaniak, M. J. *Nanotechnology* **2013**, *24* (50), 505302.

(99) Wang, S.-H.; Liang, M.-T.; Chang, C.-C.; Liao, C.-H.; Chen, C.-Y.; Chen, Y. P. Method for Preparing Radioactive-Substance Adsorbent Depositing on a Carriable Structure. US 2011/0130274 A1, 2011.

(100) Brina, R.; Miller, A. *Anal. Chem.* **1992**, No. 20, 1413–1418.

(101) Wellman, A. D.; Sepaniak, M. J. *Anal. Chem.* **2007**, *79* (17), 6622–6628.

Appendix

This appendix has been reprinted with permission from

Supporting Information

Retention in Porous Layer Pillar Array Planar Separation Platforms

Danielle R. Lincoln, Nickolay V. Lavrik, Ivan I. Kravchenko, and Michael J. Sepaniak

Analytical Chemistry **2016** *88* (17), 8741-8748

DOI: 10.1021/acs.analchem.6b02079

Determination by simple modeling of surface area increase due to PSO deposition

Each pillar was assumed to be a cylinder with a height of 20 um and a radius of 1 um. The PSO coating was then assumed to be a close-packed arrangement of spheres around this cylinder, adding 0.05, 0.1, or 0.15 um to the cylinder radius depending on the thickness of PSO deposited. Figure A-1 illustrates this model.

The volume of PSO, V_{PSO}, was calculated by subtracting the volume of the smaller cylinder, without PSO, from that of the larger cylinder. The volume of PSO that is not void, V_{porous}, was then calculated using the 34% void fraction determined by ellipsometry

$$V_{porous} = V_{PSO} * (1 - void\ fraction). \qquad (1)$$

The volume of one sphere, $V_{1sphere}$, was calculated by assuming that one PSO granule has a radius of 0.0025 um. This allowed us to calculate the number of spheres present, $N_{spheres}$, using

$$N_{spheres} = \frac{V_{porous}}{V_{1sphere}}. \qquad (2)$$

The surface area of all the spheres, A_{porous}, could then be calculated by

$$A_{porous} = A_{1sphere} * N_{spheres} * Rg, \qquad (3)$$

where $A_{1sphere}$ is the surface area of one sphere, assuming a radius of 0.0025 um, and R_g is a surface roughness factor assumed to be 3. This value could then be compared to the surface area of the small pillar, A_{pillar}, by computing a ratio

$$increased\ area = \frac{A_{porous}+A_{pillar}}{A_{pillar}}. \qquad (4)$$

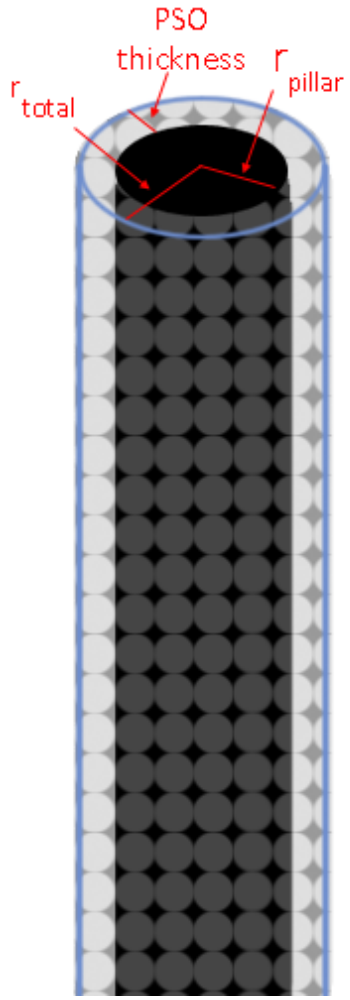

Figure A-1: Depiction of the model used to calculate surface area increase.

Vita

Danielle was born in Miami, FL in June 1990. She attended the zoo magnet program at Richmond Heights Middle School, which began her long love affair with science. After graduating high school, she moved north to Orlando to attend Rollins College, where she was introduced to Analytical Chemistry. She took the opportunity to participate in undergraduate research on the detection of gun shot residues by ultra-performance liquid chromatography/mass spectrometry (UPLC/MS) at Florida International University under Dr. Bruce McCord. Danielle graduated from Rollins with honors in May 2012. That same year, she accepted a graduate assistantship at the University of Tennessee, Knoxville in the Chemistry Department and subsequently joined the research group of Dr. Michael Sepaniak. She will graduate with her Ph.D. in May 2017.